A Spatiotemporal Profile of Visual System Activation Revealed by Current Source Density Analysis in the Awake Macaque

Charles E. Schroeder[1,2,3], Ashesh D. Mehta[2] and Syndee J. Givre[2]

[1]Program in Cognitive Neuroscience and Schizophrenia, Nathan Kline Institute for Psychiatric Research and Departments of [2]Neuroscience and [3]Neurology, Albert Einstein College of Medicine, Bronx, New York, USA

We investigated the spatiotemporal activation pattern, produced by one visual stimulus, across cerebral cortical regions in awake monkeys. Laminar profiles of postsynaptic potentials and action potentials were indexed with current source density (CSD) and multiunit activity profiles respectively. Locally, we found contrasting activation profiles in dorsal and ventral stream areas. The former, like V1 and V2, exhibit a 'feedforward' profile, with excitation beginning at the depth of Lamina 4, followed by activation of the extragranular laminae. The latter often displayed a multilaminar/columnar profile, with initial responses distributed across the laminae and reflecting modulation rather than excitation; CSD components were accompanied by either no changes or by suppression of action potentials. System-wide, response latencies indicated a large dorsal/ventral stream latency advantage, which generalizes across a wide range of methods. This predicts a specific temporal ordering of dorsal and ventral stream components of visual analysis, as well as specific patterns of dorsal–ventral stream interaction. Our findings support a hierarchical model of cortical organization that combines serial and parallel elements. Critical in such a model is the recognition that processing within a location typically entails multiple temporal components or 'waves' of activity, driven by input conveyed over heterogeneous pathways from the retina.

Introduction

A visual scene is analyzed through a sequence of fixations and saccades. Each fixation initiates a volley of retinal input that courses through the subcortical pathways and through multiple stages of cortical processing into the 'dorsal' and 'ventral' streams of the parietal and temporal lobes (Ungerleider and Mishkin, 1982; Merrigan and Maunsell, 1993). During periods of stable fixation, additional volleys of activity are sent into the system by changes in elements of the scene, such as movements or color/luminance contrast shifts. Given these dynamics, it is of interest to define precisely the spatiotemporal pattern of the visual system's response to a visual input

The transit of a volley of retinal input through a particular cortical area can be described by the local laminar activation profile. Anatomical findings predict a characteristic 'feed-forward' laminar activation profile (Rockland and Pandya, 1979; Felleman and Van Essen, 1991), with initial activation centered on Lamina 4, followed by activation of extragranular laminae. Within V1, the laminar activation sequence appears invariant and in conformity with anatomic predictions (Mitzdorf and Singer, 1979; Mitzdorf, 1985; Kraut *et al.*, 1985; Schroeder *et al.*, 1990a, 1991; Maunsell and Gibson, 1992; Lamme *et al.*, 1993; Givre *et al.*, 1994, 1995), despite the fact that the timing and laminar distribution of activity is clearly affected by lesioning of specific afferent channels (e.g. Maunsell and Gibson, 1992), variation in stimulus parameters (Schroeder *et al.*, 1991; Givre *et al.*, 1995) and local pharmacologic manipulation (Connors, 1984; Schroeder *et al.*, 1990a, 1997a). However, some cortical areas, such as V4, may not adhere to the excitatory feedforward scheme (Givre *et al.*, 1994).

The transit of a retinal volley through the different regions of the visual pathways can be described through the temporal activation profile of the cerebral cortex, or in other words, the order and time frame of cortical activation. In broad terms, such information can specify the dynamics of visual information processing, for example, by firmly establishing the time required for inputs to reach the upper areas of the visual hierarchy (e.g. Donders, 1968). In specific terms, response latency measures can play a key role in a 'functional connectivity analysis'. In this case, onset latency measures are used to define the activation sequence across laminae in particular structures (Mitzdorf and Singer, 1979; Best *et al.*, 1986; Schroeder *et al.*, 1991; Maunsell and Gibson, 1992; Givre *et al.*, 1994; Bullier and Nowack, 1995; Nowak and Bullier, 1995), and across structures comprising the system (Raiguel *et al.*, 1989; Maunsell, 1987; Givre *et al.*, 1994; Nowak *et al.*, 1995; Bullier and Nowack, 1995; Munk *et al.*, 1995). A less common use of latency measurements is to aid in determining the neural origins of human event-related potential (ERP) components (e.g. Robinson and Rugg, 1988; Givre *et al.*, 1994; Schroeder *et al.*, 1994). Both of these applications can be distinguished from ones designed to determine the nature of the information encoded in the temporal activity patterns of single neurons (Richmond and Optican, 1987; Optican and Richmond, 1987; Richmond *et al.*, 1987; McClurkin *et al.*, 1991, 1996; McClurkin and Optican; 1996; Victor and Purpura, 1996).

The present study falls primarily in the category of functional connectivity analysis. We evaluated temporal activation patterns within specific cortical regions, and across the visual system as a whole, in the awake monkey, by measuring responses elicited by one standard visual stimulus, at points throughout the pathways. Although the more common practice is to optimize stimulation for neuronal response properties within each area, this precludes direct comparison of responses across areas, and thus one cannot determine how a given stimulus activates an observer's visual system as a whole. Use of a standardized stimulus overcomes this difficulty and, in conjunction with those of other laboratories, our findings provide a step in establishing a generalized spatiotemporal pattern of visual cortical activation. Neuronal ensemble responses to visual stimuli were analyzed using laminar current source density (CSD) and multiunit activity profiles, sampled with linear array multielectrodes, positioned to span the cortical laminae at each recording site (Schroeder *et al.*, 1991). Although it was usually possible to corroborate CSD measures of neural response with co-located multiunit activity, the main analyses used the CSD measure. CSD analysis entails a second-derivative approximation of the voltage gradient from a profile of field potentials, in the present case, visually evoked potentials (VEPs). CSD analysis defines the laminar profile of transmembrane current flow, and

thus the timing and laminar distribution of synaptic inputs whether or not they produced concomitant action potentials (e.g. in the case of subthreshold and modulatory inputs — see Schroeder *et al.*, 1994, 1995; Schroeder, 1995). The major use of the action potential measures in this study was to aid in defining CSD components as indices of excitation and inhibition.

An ancillary goal of these studies was to provide information relevant to the physiological interpretation of results obtained with event-related potential (ERP) measures in humans (e.g. Allison *et al.*, 1994; Foxe *et al.*, 1994; Halgren *et al.*, 1994). The methods of the present study produce measurements directly comparable to ERP and related magnetoencephalographic (MEG) measures (see e.g. Schroeder *et al.*, 1994; Schroeder, 1995). Our findings are, however, of general interest for non-invasive neuroimaging studies in humans, particularly those using methods with poor temporal resolution, such as positron emission tomography (PET) and functional magnetic resonance imaging (fMRI) (Ungerleider, 1995). They illustrate how, under specified conditions, we can index the order and overall 'time frame' of cortical activations produced by sensory inputs, at an ensemble level of analysis appropriate for defining the brain structures and neural processes reflected in an activation focus.

Materials and Methods

Subjects

Nine male monkeys (*Macaca fascicularis*), weighing between 3.5 and 5.5 kg, were subjects in these experiments. Each monkey also served in at least one other experiment in which recordings were obtained from visual, somatosensory or auditory cortices. All procedures were approved by the Institutional Animal Care and Use Committee, and conformed to the Principles of Laboratory Animal Care (NIH Publication no. 86–23, revised 1985).

Surgical Preparation

Preparation of the subjects for chronic recording was performed using aseptic techniques, under general anesthesia (sodium pentobarbital 25.0 mg/kg). Throughout surgery, the rectal temperature and respiration rate were continuously monitored and maintained within physiological limits. Perioperative care included the use of systemic analgesics, local and systemic antibiotics, and parenteral fluid replacement. The monkey was positioned in a stereotaxic instrument, the skin and fascia overlying the calvarium were resected and appropriate portions of the skull were removed. To provide electrode access to the brain, groups of 80–100 stainless steel tubes (18 gauge), glued together in a parallel matrix, were sealed with surgical grade silastic and implanted over the cortex of interest, in contact with the intact dura. Matrices were positioned normal to the brain's surface for orthogonal penetration of areas V1 and V4. Individual epidural guide tubes were positioned overlying central and frontal sites to serve as fixed ground and reference electrodes. The matrices, monitors and Plexiglas bars with sockets (to permit painless head restraint) were secured to the skull with stainless steel screws embedded in dental acrylic. A recovery time of 2 weeks was allowed prior to the beginning of data collection. Data were collected with the monkey comfortably seated in a primate chair in an electrically shielded, darkened, sound-attenuated chamber.

Visual Stimulation

As discussed above, optimization of stimuli for each recording location was inappropriate for the present study, because it confounds the comparison of responses across structures. Thus, while limited analyses of pattern-evoked responses are included here, we used one form of visual stimulation, diffuse light, for all main comparisons. Light flashes 10 μs in duration and 7.8×10^5 lux intensity, were generated by a Grass PS-2 photostimulator and presented at 2/s from a diffuser subtending 20° visual angle, directly in front of the animal (Schroeder *et al.*, 1990a, 1991). A speaker driven by a white noise generator was used to mask the click of the lamp discharge and extraneous noise. Although, in many cortical units, responses to diffuse light flash are moderate to poor in quality, when activity is measured with CSD and multiunit activity profiles, flash-evoked responses are robust in both P and M laminae of LGN (Schroeder *et al.*, 1989; 1990a, 1992), in cortical areas V1 (Kraut *et al.*, 1985; Mitzdorf and Singer, 1979; Schroeder *et al.*, 1990a, 1991) and V4 (Givre *et al.*, 1994), and throughout the higher cortical visual areas (present results). More importantly, flash stimulation presented several unique advantages for the present study. First, because of its intensity and its sharp rise and fall, light flash elicits impulse responses in cortical ensembles with correspondingly sharper onsets than those to other common forms of stimulation (see e.g. Fig. 6) and the longer latency activity is not complicated by stimulus offset responses. Such responses are most amenable to quantitative analysis. Second, due to both the supramaximal intensity of this stimulation and to the large degree of light scatter, stimulation is relatively constant over a wide range of eye positions, thus obviating the need for rigorous constraint of eye position or visual attention. The adequacy of flash stimulation for the quantitative study of laminar activation profiles was assessed in several ways. Preliminary experiments compared the laminar activation profiles elicited by diffuse light with those elicited by patterned flash and pattern-reversal stimulation. The patterned flash stimulus was a black and white, square-wave grating (3 cycles/degree, white bar luminance ~50 cd/m^2, contrast ~60%) presented on a video monitor subtending 4° radial to a central point, on which the monkey was required to fixate. The bar grating was presented from a dark background screen, and thus had a substantial luminance component, along with the pattern component. It was matched as closely as our equipment permitted to the stimulus used by Maunsell and Gibson (1992). Pattern reversal stimulation used the same bar grating, counterphase modulated, so that switching between phases had no luminance component. The results of this comparison, along with those of several other tests, are described at the beginning of the Results section, and the issue of choice of stimuli and its implications is revisited in the discussion.

Eye Position

Eye position was monitored in a subset of the experiments, using a Stoelting, Model 4100/4500 infrared system, with a resolution of 1.0° of visual angle. Stimulus presentation was gated so that the animal had to fixate within a small window surrounding the fixation point, in order to receive any stimulation (and the consequent opportunities for reinforcement at the point of fixation point dimming).

Recording and Signal Processing

Neural activity was assessed using laminar CSD and multiunit activity profiles, which index local patterns of PSPs and action potentials respectively (Schroeder *et al.*, 1991). To obtain these profiles, neuroelectric activity was sampled from numerous incremental depths simultaneously using linear array multicontact electrodes with intercontact spacings of 75, 100, 150 or 200 μm and contact impedances of 0.3 MΩ at 1000 Hz. Each response profile represents an averaged response to 200 stimulus presentations. The electrode is illustrated and critical points concerning activity measurements are described at the beginning of the Results section. An epidural electrode near the frontal midline or a subcutaneous needle electrode in front of the contralateral ear served as a reference. The electrode contacts were coupled via unity gain preamplifiers to Grass P5 amplifiers set at a gain of 5000 and a bandpass of 3 Hz–3 kHz (6 dB down, roll-off 6 dB/octave). For field potential recordings, the amplifier outputs were digitized at 2 kHz and averaged using a Nicolet Pathfinder minicomputer. Although this procedure can cause aliasing of high-frequency signals, analysis of power spectra (for adequately digitized signals) showed that most of the power in the signal is concentrated below 50 Hz and there is negligible power above 1 kHz. Raw signals were also recorded on analog tape (EMI SE 7000) for off-line processing. In order to derive an index of action potentials occurring in the vicinity of each electrode contact, multiunit activity was recorded and averaged in parallel with the field potentials. The amplified signal was band pass filtered (0.5–2 kHz, roll-off 24 dB/octave), full-wave rectified, further amplified (gain = 8) and digitized at 4 kHz.

CSD Derivation

The CSD profile provided the primary means of defining the laminar sequence and distribution of visually evoked activity. While it was usually possible to corroborate CSD measures of neural response with co-located multiunit activity, the main analyses of spatial (laminar) and temporal response patterns used the CSD measure in preference to multiunit activity because it is a more direct index of afferent input. That is, the transmembrane current flow measures index the PSP, which is the first-order response to synaptic input. One important consequence is the ability to assess the timing and laminar pattern of synaptic activations whether or not they directly produce net increases in action potentials (e.g. in the case of subthreshold and modulatory inputs). The action potential measures in these studies were used to help in defining co-located CSD features as indices of excitation and inhibition and to aid the comparison of our results with those of studies measuring action potentials alone. One-dimensional CSD analyses of the VEP profiles were calculated using a three-point formula for approximation of the second spatial derivative (Freeman and Nicholson, 1975):

$$D = \frac{d^2 f}{dx^2} = -\frac{\left[f(x-h) - 2f(x) + f(x+h)\right]}{h^2}$$

where f is the voltage, x is the point at which D is calculated and h is the differentiation grid. To maximize spatial resolution, numerical differentiation for calculation of the CSD uses the intercontact spacing on the electrode as its grid (h). In all recordings, electrode penetrations were made orthogonal to the local lamination pattern, in keeping with the requirements of one-dimensional CSD analysis (e.g. Mitzdorf, 1985) and assisted by pre-implant MRI (see below). Earlier experiments have established procedures for applying and interpreting CSD analysis in both cortical (Schroeder *et al.*, 1990, 1991, 1997; Givre *et al.*, 1994, 1995; Schroeder, 1995) and subcortical (Schroeder *et al.*, 1992) structures. We have explored the strengths and limitations of CSD analysis through these empirical studies in interaction with modeling and simulation experiments (Tenke and Schroeder, 1990, 1992; 1994; Tenke *et al.*, 1993). Routine analysis of CSD profiles includes a step of summing all individual traces together to determine the extent to which the outcome deviated from zero. This provided an assessment of the electrophysiological sampling underlying the derived CSD profile (e.g. the degree to which the active transmembrane current flow distribution was bracketed by the position of the recording array), as well as a means of detecting local tissue factors (e.g. conductance inhomogeneity) and electrode problems (e.g. extremely mismatched electrode impedances) which can produce artifacts in the CSD profile. See Tenke *et al.* (1993) for detailed treatment of these issues.

AVREC Derivation

To facilitate quantification and analysis of CSD data, all of the waveforms comprising the laminar CSD profile were baseline corrected with respect to the prestimulus epoch, then full-wave rectified and averaged together (Givre *et al.*, 1994). Rectification leads to loss of information regarding the direction of transmembrane current flow; however, it permits averaging of CSD waveforms without the outcome going to zero. The resulting waveform, termed the AVerage REctified Current, or AVREC waveform, provides a measure of the temporal pattern of current flow over the specific, spatial extent of tissue sampled in the penetration.

Measurement of Onset Latency

Onset latency was measured once for each electrode penetration, using the above-described AVREC measures. Specifically, latency was determined with a routine that identified the earliest significant (>2 SD units) deviation from the baseline, with the further provision that deviation from the baseline had to be maintained at or above 2 SD units for 8 out of 10 of the following sampling points (each point corresponding to 0.5 ms at the 2 kHz sampling rate); the latter was used to prevent spurious deflections from being coded as onset latencies. For each waveform, the baseline SD was determined using a prestimulus period of at least 20 ms duration. The epoch extending from 5 ms prestimulus to 10 ms poststimulus was excluded from analysis in order to eliminate contamination from stimulus artifacts. Statistical comparisons of latency distributions across areas used a nonparametric Kolmogorov–Smirnov analysis (Daniel, 1978).

MRI-assisted Targeting of Electrode Penetrations

Specific visual areas were targeted by anatomical location. Targeting in each animal used a stereotaxic approach, customized for the animal's unique anatomical variations, using MRI, obtained prior to surgical preparation (Schroeder *et al.*, 1994). During scanning, that monkey was immobilized for ~1.5 h using sodium pentobarbital (i.v., 12–15 mg/kg). Cranial MRI were obtained using a Signa Performance Plus 1.5 T MR scanner (General Electric, Milwaukee, WI). A coronal T_2-weighted spin echo sequence was performed (T_R = 4000, T_E = 30.90 ms, 256 × 256 matrix, rectangular 14 cm FOV, one excitation, 3 mm interleaved), followed by a T_1-weighted, three-dimensional spoiled gradient echo sequence (T_R = 55, T_E = 17, θ = 60°, 256 × 192 matrix, 12 cm FOV) providing 60 continuous 1 mm sections. The former enhanced tissue contrast and the latter produced thin sections for subsequent reformation and three-dimesnional display. The post image processing was performed on a Sun SPARCStation 370 workstation (Sun Microsystems, Mountain View, CA) with direct Ethernet linkage to the Signa. This method presents a critical improvement over the use of stereotaxic atlas coordinates in the accuracy of targeting brain structures. Locations of brain structures were translated into stereotaxic coordinates by their relationship to the bony landmarks that define the stereotaxic plane, the external auditory meatus and the infraorbital rim. Thus, both location of target structures and angles of electrode penetrations with respect to stereotaxic coordinates and planes of reference were precisely defined. Such targeting of electrode penetrations orthogonal to the cortical surface within deep sulci, and with reference to the vertical and horizontal stereotaxic planes, is illustrated in Figure 1. As stated above, precise targeting is important in maximizing the application of one-dimensional CSD analysis.

Histological Reconstruction

Anatomical confirmation of recording sites was the definitive means of identifying specific visual areas and it permitted elimination of data from penetrations that crossed cortical laminae at extreme angles. Such penetrations were usually obvious on functional grounds because the active region could not be straddled with a recording array extending over 2 mm. Electrode penetrations were reconstructed in postmortem histology, as illustrated in Figure 2. During some electrode penetrations, lesions were made by passing current through one electrode contact. At the end of data collection, each monkey was deeply anesthetized and perfused through the heart with buffered physiological saline followed by 5 or 10% buffered formalin. The brain was removed and cut into 40, 80 or 120 μm sections, parallel to the plane of electrode penetration. Sections were stained with potassium ferricyanide to facilitate the location of electrode tracks and iron deposits, and counterstained with cresyl violet. With few exceptions, we were able to reconstruct the entire pattern of penetrations in a given region, because the electrode penetrations were rigidly confined to a grid defined by the guide tube matrix.

Functional Positioning of the Electrode Array

After using the procedures described above to determine stereotaxic location and electrode penetration angle for a particular target region, further positioning of the depth of the linear contact array on the electrode was based on the local electrophysiological activity patterns, as illustrated in the next section (see Fig. 4). Functional guidance of the penetration exploited the fact that all visual areas we have studied to date generate a field potential distribution that volume conducts with a relatively constant rate of amplitude decay (i.e. second derivative approaches zero) over distances from the active region (see e.g. Schroeder *et al.*, 1994). Visually evoked activity profiles were collected at successive depths beginning well in advance of the expected depth of the target region. Linear amplitude increase (i.e. a near-zero second derivative) indicated approach to an active visual area. Arrival at the depth of the active region was indicated by the appearance of steep acceleration in the field potential gradients and/or component polarity inversions (i.e. a non-zero second derivative). The reason that acceleration in the voltage gradient or frank polarity inversion of a component is important is that

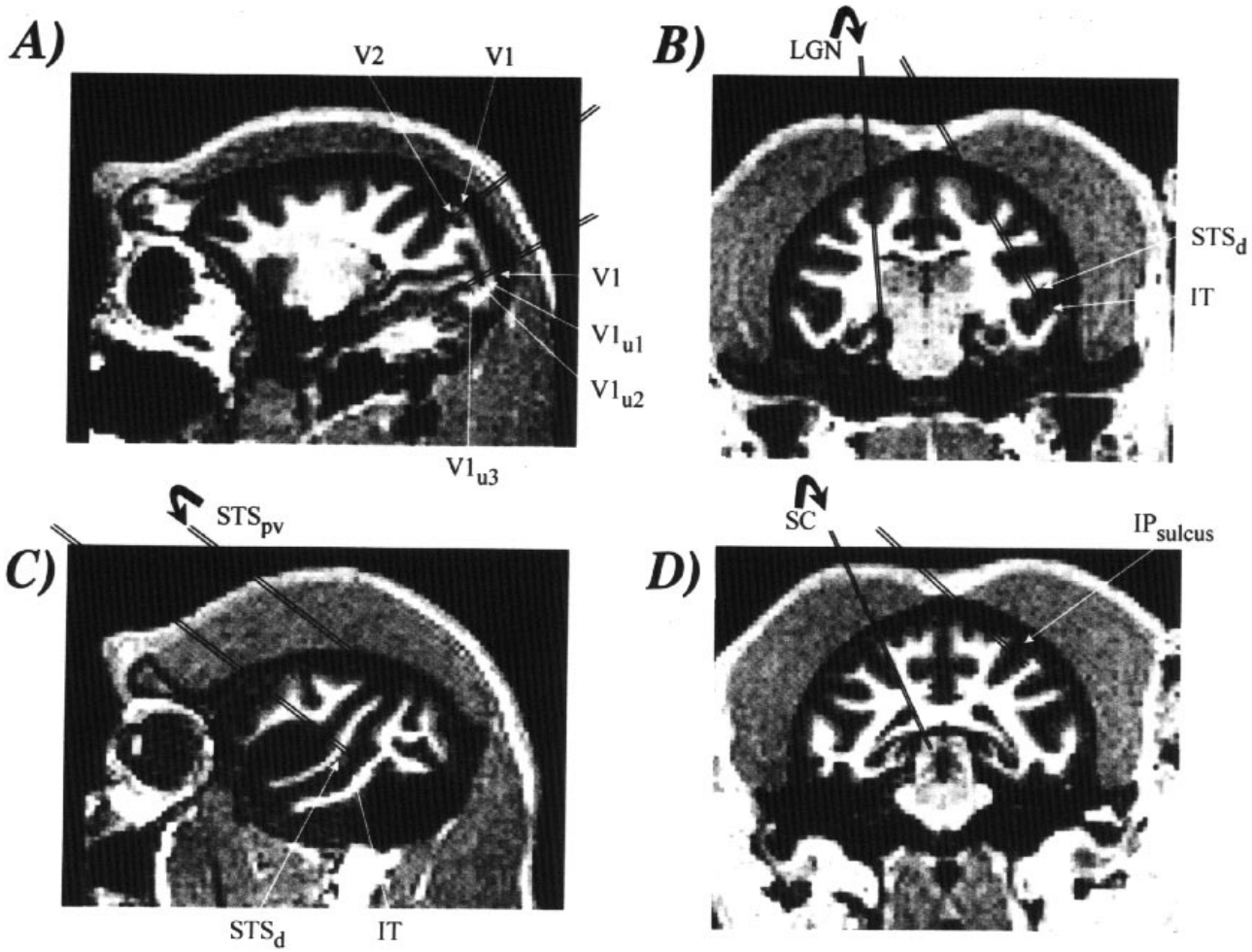

Figure 1. (*A*) A parasaggital MRI slice through the brain of one subject showing the electrode targeting of posterior visual areas. Superimposed double lines depict the preferred sampling approaches for each area. V1 was sampled primarily in the lateral opercular surface (upper) to access the foveal and parafoveal representations of the visual field. The exception to this is that, in a minority of cases, penetrations were made into the medial–ventral operculum, sampling from the surface and underlying belts of V1 tissue (see lower) in order to access the more peripheral visual field representations. V2 was accessed mainly by penetrating through V1 in locations immediately posterior to the lunate sulcus (upper). V4 was approached mainly by penetrating directly into the prelunate gyrus (not illustrated). (*B*) A coronal MRI slice illustrating the approaches to LGN (left) and to visual areas STSd and IT (right), located in the upper and lower banks respectively of the anterior portions of the superior temporal sulcus (STS). It is emphasized that use of the different penetration angles was important for optimal implementation of one-dimensional CSD analysis. (*C*) a saggital MRI slice showing the A–P angle used for recording from STSd and IT (lower) and STSpv (upper). (*D*) A coronal MRI slice showing the penetration angles for superior colliculus (SC, left) and visual regions both banks of the intraparietal sulcus (collectively referred to as IP, right). See text for additional details on definition of visual areas

these perturbations in the voltage gradient are observed at points where there is a net inward or outward current flow. In other words, transmembrane current flow is the main origin of the field potential distribution in the extracellular medium, and approximation of the second derivative of voltage, through CSD analysis, permits estimation of the macroscopic pattern or local profile of net inward (sink) and outward (source) transmembrane current flow (e.g. Mitzdorf, 1985). Multiunit activity was also used to help in positioning the electrode array. Multiunit activity, in association with a relatively flat CSD profile, indicated that the electrode array was traversing a span of white matter. Sulcal cortical visual areas and subcortical structures such as LGN and superior colliculus were distinguished from intervening white matter regions by the conjunction of large CSD components with multiunit activity (Givre *et al.*, 1994). Since the CSD indexes the net local transmembrane current flow that attends synchronous synaptic activation within cortical or subcortical structures, the large, current-balanced CSD profiles characteristic of cortical regions and laminated nuclear structures are not found in association with the multiunit activity recorded in white matter (see Fig 4*a*; see also Schroeder *et al.*, 1995b). After localizing an active region, further depth adjustments were made based on the CSD profile so as to straddle its laminar expanse with the electrode array. Because the uppermost laminae in most cortical areas were relatively quiescent, under the conditions of this study, we were able to distinguish and study sulcal areas whose pial surfaces were opposed (e.g. areas within the internal folds of V1 — Fig. 4, and those within the IP sulcus). In any case, the outer boundaries of an active cortical region, both pial and white matter, are indicated by drops to near-zero CSD values. Then, after the direction from which the tissue was penetrated (pial or white matter) is determined (by track reconstruction), approximate internal laminar assignments could be made, based on the known internal geometry of the region (see below).

Definition of Visual Areas

Visual areas were defined by anatomical location and, in certain cases, by physiological characteristics (Schroeder *et al.*, 1991; Givre *et al.*, 1994). All identification was subject to histological verification. The cortical areas we sampled, along with relevant electrode penetration angles, are illustrated using one subject's MRI in Figure 1. Examples of electrode

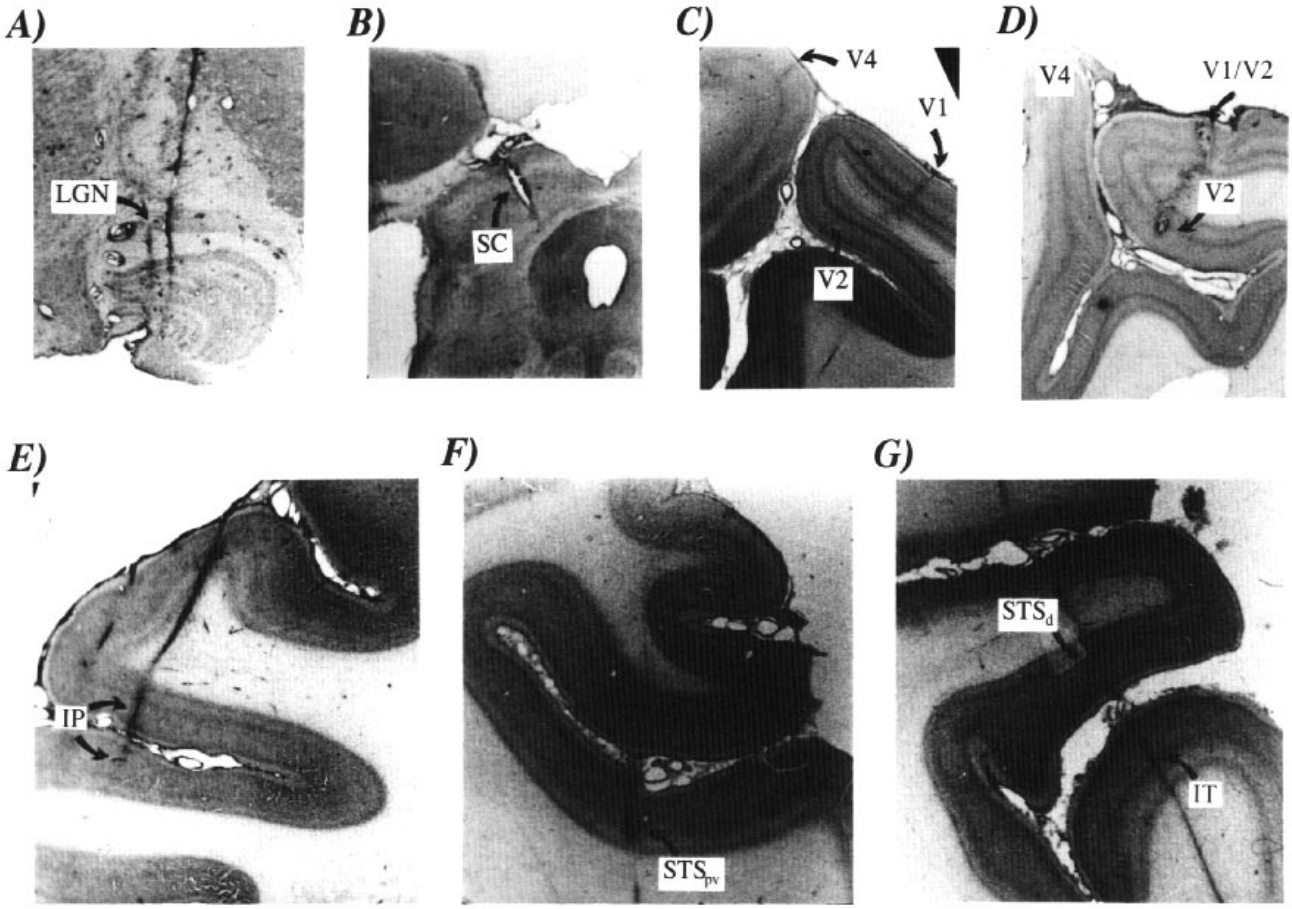

Figure 2. All material shown here consists of Nissl-stained, 80 μm sections. Electrode tracks shown here were from penetrations made at the angles illustrated in Figure 1. (*A*) A coronal section through the LGN in one subject, showing two electrode tracks. (*B*) A coronal section through the superior colliculus in one subject showing a lesion made during a recording penetration. (*C*) a parasaggital section through the right operculum of one subject, showing penetrations through V1 (right), V2 (lower) and V4 (upper). The V1/V2 border is evident at the brain surface approximately between the V1 and V4 penetrations. An additional track in the white matter below V2 is also visible at the bottom. (*D*) a similar section from another subject showing lesions made in the superficial laminae at the V1/V2 border (upper) and in Lamina 4 of V2 (lower). (*E*) a coronal section through the region of the anterior intraparietal (IP) sulcus showing two electrode tracks. Medial and lateral bank areas are grouped together as Area IP in the present study. Coronal sections in (*E*)–(*G*) were cut at ~30–40° anterior of stereotaxic vertical, to approximate the angle of penetration (see Fig. 1*C*). (*F*) A coronal section through he posterior superior temporal sulcus showing an electrode track and lesion in the ventral bank of the STS, which at this A–P level, is termed STSpv. The posteriormost portion of the lateral sulcus is visible immediately above the STS. (*G*) A coronal section through a more anterior location in the STS showing an electrode track through upper and lower bank areas, termed STSd and IT respectively. See text for additional details on area designations.

track reconstructions for each area are provided in Figure 2. Subcortical recordings were obtained in four animals. For LGN, to optimize the use of one-dimensional CSD analysis, data were taken from recordings in the crown and medial wing of LGN (see Schroeder *et al.*, 1992); with appropriate angles, penetrations were made orthogonal to the lamination patterns and P and M laminae were sampled concurrently (Figs 1*B* and 2*A*). P and M laminae in LGN were distinguished as in previous studies (Schroeder *et al.*, 1989, 1990b, 1992). Superior colliculus was sampled in one subject using an appropriate medial–lateral angle (Figs 1*D* and 2*B*). V1 recordings were obtained from the lateral surface of the striate operculum (Figs 1*A* and 2*C*,*D*), except that in one animal additional recordings were obtained from the underlying belts of V1 tissue in the medial–posterior operculum (e.g. Fig. 1*A*: $V1_{u1,\ u2...}$). V2 recordings were made primarily in the first belt of cortical tissue underlying the operculum, immediately posterior to the lunate sulcus, by penetrating through V1 (Figs 1*A* and 2*C*,*D*). V4 recordings were in the crown of the prelunate gyrus (Fig. 2*C*). Recordings within superior temporal sulcus (STS) were grouped into three divisions: (i) STSd (**d**orsal), primarily area STP (Figs 1*B*,*C* and 2*G*), (ii) STSpv (**p**osterior to the lateral sulcus, **v**entral bank of STS), including MT and immediate surrounds (Figs 1*C* and *2*F), and (iii) IT (ventral bank of STS, underlying the lateral sulcus), primarily inferotemporal cortex (Figs 1*B* and 2*G*). Recordings from both banks of the intraparietal (IP) sulcus were grouped together in area IP (Figs 1*D* and 2*E*).

Identification of Laminae

Laminar identifications in V1 could be made with confidence based on intracortical physiology, because of our prior, extensive confirmation of VEP component inversion depths from reconstruction of electrode tracks and lesions (see Fig. 2 above; Kraut *et al.*, 1985, 1991; Givre *et al.*, 1994). In V1 penetrations in the present study, the center of the electrode array was offset slightly above the base of lamina 4c as defined by the inversion point of the flash-evoked N40 component (see Schroeder *et al.*, 1991). In the extrastriate areas, our laminar identifications are based on a combination of the lesion–physiology correlations we have confirmed to date. Our confidence levels for laminar identifications in the various regions are stated in declining order as follows. In V4, prior work by Givre *et al.* (1994) showed that the position of Lamina 4 is reliably indicated by the polarity inversion point of the N95 VEP component (see Fig. 9). The N95 inversion is attended by a current sink and a correlated multiunit response reflecting the feedforward input from V1 and V2. As was shown for V1, in V2 and in the dorsal stream areas, the earliest local response appears as a robust excitatory configuration (current sink and multiunit activity increase), located immediately below the middle of the local

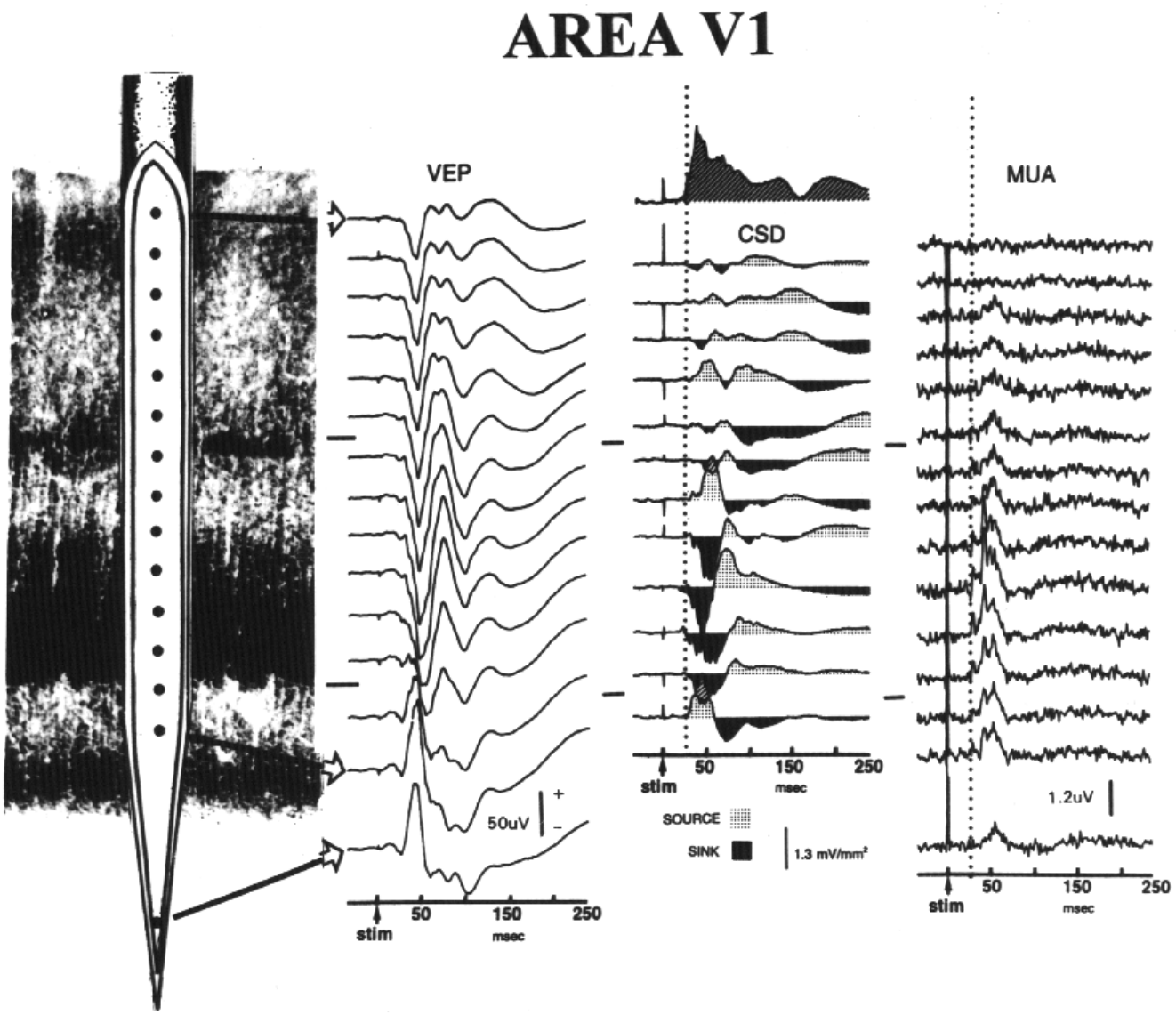

Figure 3. A laminar activity profile consisting of visual evoked (field) potentials (VEPs), current source density (CSD) and multiunit activity (MUA) recorded simultaneously across the middle and upper laminae of V1 using a multicontact electrode with intercontact spacings of 100 mm. The electrode had a contiguous array of 14 contacts covering a distance of ~1.3 mm, with a 15th (probe) contact located 1 mm below the main array. Probe recordings in the subjacent white matter are displayed below the VEP and MUA columns. Laminar locations are indicated in the left margin. To illustrate the recording preparation, the electrode is shown scaled and positioned with respect to the cytochrome oxidase anatomy of striate cortex (left). Shown at the top of the CSD profile is the averaged rectified current flow (AVREC) waveform, obtained by full-wave rectifying all of the traces in the CSD profile and averaging them together. Drop lines in the CSD and MUA columns indicate the onset latency as determined by the statistical criteria used in this study (see Materials and Methods).

laminar expanse. This location matches the expected position of Lamina 4, given the expanded size of the supragranular laminae in extrastriate areas, relative to V1 (see e.g. Hendry *et al.*, 1990; Jones, 1990). While not yet confirmed directly for all dorsal stream areas, lesion–physiology correlations verified to date (e.g. in V2, Fig. 2*D*; STSpv, Fig. 2*F*) support this assignment. Laminar assignments in IT are regarded with least confidence at present, partly because we have not yet recovered lesions sufficiently small to permit precise laminar localization, and partly because the initial response in IT usually does not contain prominent excitatory CSD and multiunit activity configuration that would help to localize Lamina 4 (see also Givre *et al.*, 1994). Even in this case, however, the width of the active region, as indexed by its CSD profile, corresponds to the dimensions of the cortex, and thus the gross laminar assignments depicted in Figures 10 and 11 can be approached with some degree of confidence.

Results

The results are organized in four sections. Section 1 addresses the physiological interpretation of the laminar activation profile, description of the electrophysiological patterns that enable functional positioning of the electrode array in visual areas, and the qualities of diffuse light stimulation in the context of laminar activity profile analysis. Sections 2 and 3 describe and contrast the laminar activation profiles characteristic of the dorsal and ventral stream areas. Section 4 addresses the quantified temporal activation profile across the system.

1. Light-evoked Laminar Activity Profiles

Figure 3 displays a laminar activity profile acquired from V1 using an electrode array with a 100 μm intercontact spacing.

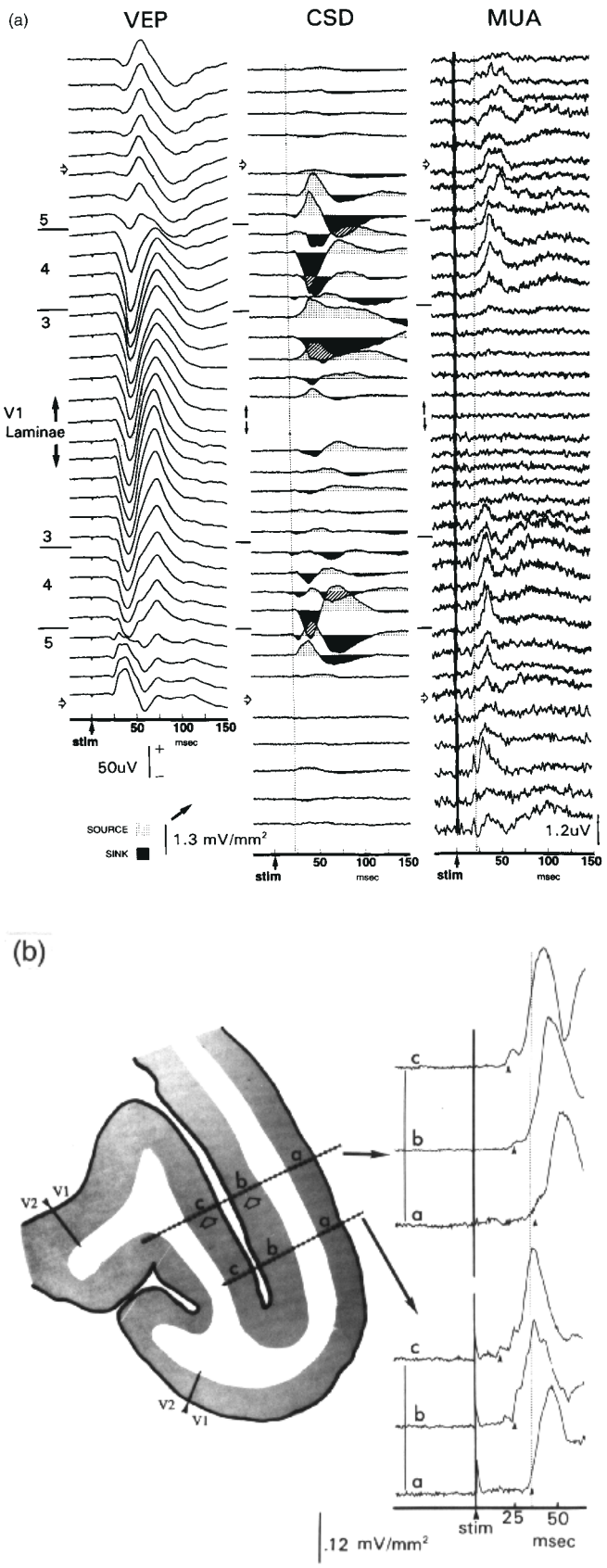

Figure 4. (*A*) Laminar activity profiles consisting of visual evoked potential (VEP), current source density (CSD) and multiunit activity (MUA) profiles, sampled from four successive, nonoverlapping depths beneath the medial posterior operculum. The junctures between the sampling positions are indicated by gaps in the CSD profile (center) and reconstruction is illustrated in (*B*). Filled arrows indicate the juncture of the opposed pial surfaces of two deep belts of V1. The open arrows indicate the grey/white matter boundary for each region. The intercontact spacings on the electrode were 150 mm and it had a contiguous array of 14 contacts. The upper belt of V1 tissue was penetrated from its white matter aspect and the lower, from its pial surface. Timing lines were placed at the onset of activity as determined from the CSD in the deeper electrode position. Other conventions are the same as in Figure 3. (*B*) Reconstruction of the penetration described in (*A*) (upper line, double arrows), along with the reconstruction of an adjacent electrode penetration. Shown at the right are AVREC waveforms derived from the laminar CSD profile at each of the sampling positions from surface to deepest belt (a–c) indicated in the reconstruction. Sites (b) and (c) in the upper track (open arrows) correspond to the locations from which the intracortical profiles in (*A*) were sampled. Drop line is placed at the onset of activity in the lowest AVREC trace. The onset of activity in each of the other AVRECs is indicated by a filled arrowhead.

Although the 100 μm spacing provides improved resolution of small laminar subdivisions in V1, it reduces the linear distance across which the array can sample activity. Because of this limitation, our V1 recording positions are often biased toward the pial surface of cortex, in order to optimize the resolution of the main input and ascending output laminae (Schroeder *et al.*, 1990a; Givre *et al.*, 1994). Profiles from electrode positions more adequately spanning the V1 laminae (at 150 μm intercontact spacing) are shown in Figure 4*A*. Depicted are laminar activity profiles from a series of electrode positions that straddled the first and second deep belts of V1 (underlying the medial operculum), as well as activity profiles from white matter regions subjacent to each belt of cortex. These regions, which are parallel to the outer surface of V1, contain representations of peripheral visual space (Daniel and Whitterage, 1961).

A reconstruction of the electrode penetration is depicted in Figure 4*B*. These figures illustrate three main points. First, as shown by numerous earlier studies (e.g. Mitzdorf and Singer, 1979; Kraut *et al.*, 1985; Schroeder *et al.*, 1990a, 1991; Maunsell and Gibson, 1992; Lamme *et al.*, 1993; Givre *et al.*, 1994, 1995), the laminar activation sequence is characteristic for V1. Initial prominent responses occur in the major thalamo- recipient laminae, followed by responses in the extragranular laminae. Variations in the appearance of this activation sequence stem from both the resolution scale of our measurement techniques and the well-noted variations in the anatomic patterns of axonal terminations, as elaborated below. Despite these factors, the regularity of the laminar activation profile within and across most visual areas is remarkable: the biggest excitatory response occurs first in and near the granular (ascending input) laminae and the prominent responses of the extragranular laminae follow this. The profiles in Figures 4 and 6*A* show the same sequence as that in Figure 3, but with less resolution (150 μm intercontact spacing). While responses in the 4C subdivisions are not as well resolved as in Figure 3, the laminar expanse of V1 is better sampled. Second, in both granular and supragranular laminae, the initial response is excitatory, as indicated by the current sinks (signaling net local depolarization) and the associated increase in multiunit activity. This is the laminar response profile predicted by the anatomy of feedforward connections (preferentially targeting in and near Lamina 4), and it is therefore referred to as a 'feedforward' laminar profile. Earlier studies (Maunsell and Gibson, 1992; Givre *et al.*, 1994) reported a noticeable (8–15 ms) lag between responses in the thalamorecipient and upper laminae. This lag is not obvious on the time-base used for Figure 3, but is clear with quantification of granular and supragranular latencies (see below, Fig. 14). Finally, consistent with earlier findings (e.g. Schroeder *et al.*, 1990a,

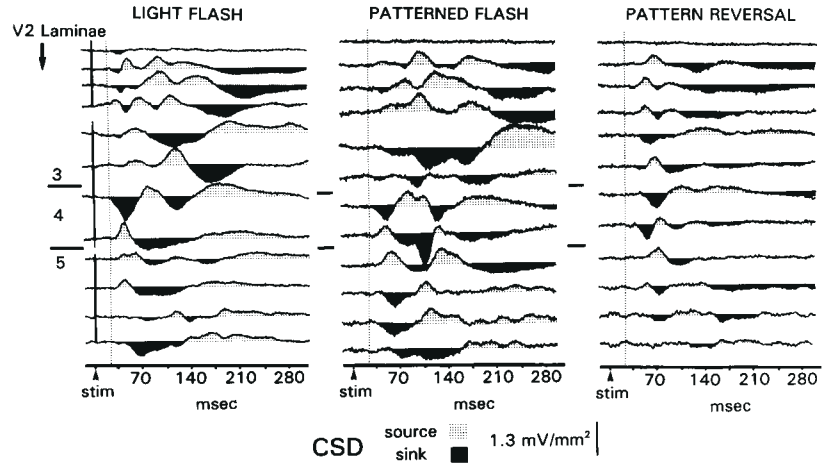

Figure 5. Laminar CSD profiles in response to the typical diffuse light stimulus (left), a pattern/flash (middle) and pattern reversal (right). These data were recorded successively from one electrode site in V2 (150 mm intercontact spacings). Pattern/flash and pattern reversal used the same stimulus, a 3 c/d vertical bar grating, black and white (square-wave spatial luminance profile), with a contrast of ~60% and white bar luminance of ~50 cd/m^2. For pattern/flash, the stimulus was presented from a dark background, while for pattern reversal, the stimulus was counterphase modulated, so that there was no overall luminance change between phases. Stimulation rates were 2/s and 1/s for diffuse light and pattern stimuli respectively. Drop lines were placed at the onset of the flash-evoked CSD as determined from the profile on the left.

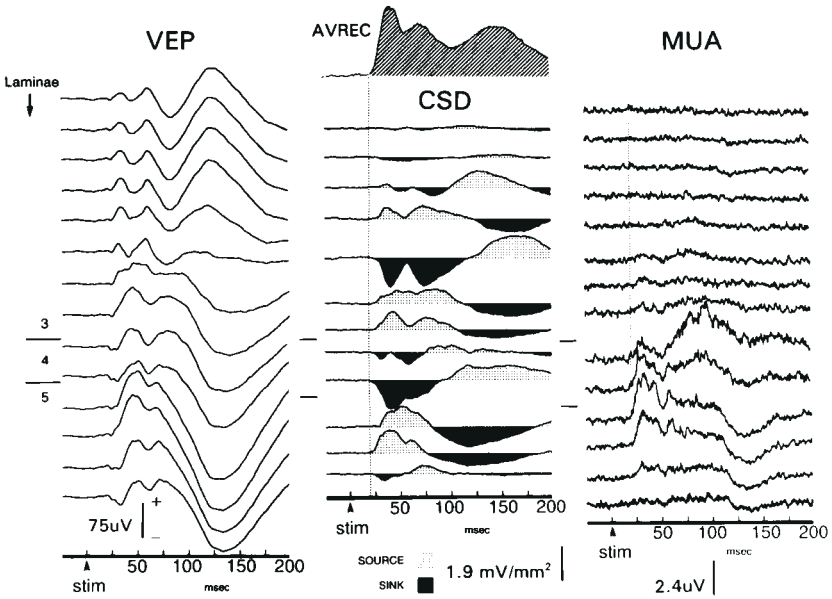

Figure 6. A laminar activity profile from STSpv using a multielectrode with intercontact spacings of 150 mm. Conventions are the same as in Figure 3.

1991; Givre *et al.*, 1994), local activity in V1 is likely to contribute to the early N40 and P55–80 components of the surface visual ERP, as indicated by the local polarity inversion of these components in V1.

The response profiles in Figures 3 and 4 illustrate the generality of the above-described light-evoked laminar activation sequence in V1, as well as the degree of variability of the later activity, especially in the supragranular laminae. Some apparent variations in the fine structure of the laminar activation profile are also due to the use of electrodes with differing intercontact spacings. As mentioned above, for example, the Lamina 4 current sinks in Figure 3 were sampled with 100 μm intercontact spacing and are better resolved than those in either Figure 4 (upper or lower) or 6A, which were sampled at 150 μm spacing. The stimulus sensitivities of the upper and lower Lamina 4C sinks show that they receive input from M- and P-type thalamic afferents respectively (Givre *et al.*, 1995). The reliability of the cortical activation sequence, coupled with the variability of later activity, particularly in the extragranular laminae, is a recurring observation across the cortical areas we have studied to date (see below). For the purpose of the present study, the important point is that in the cortical and subcortical visual areas studied to date, including LGN, V1, V2 and V4, the CSD profile reliably describes a predictable sequence of synaptic activation elicited by diffuse light, and does so in a way that can be related to cellular activity.

The basis for functional positioning of the electrode array (see Materials and Methods) is also illustrated by data in Figure 4. The critical points in this regard are: (i) visually driven synaptic activation results in transmembrane current flow, generating a

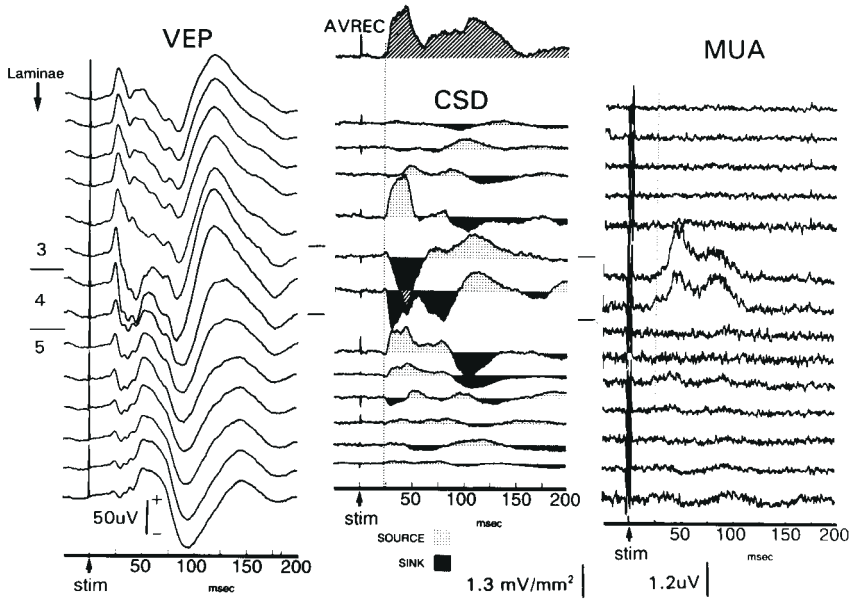

Figure 7. A laminar activity profile from the medial bank of the IP sulcus, using a multielectrode with intercontact spacings of 150 mm. The profile is displayed pial surface up, although the area was penetrated from its white matter aspect. Conventions are the same as in Figure 3.

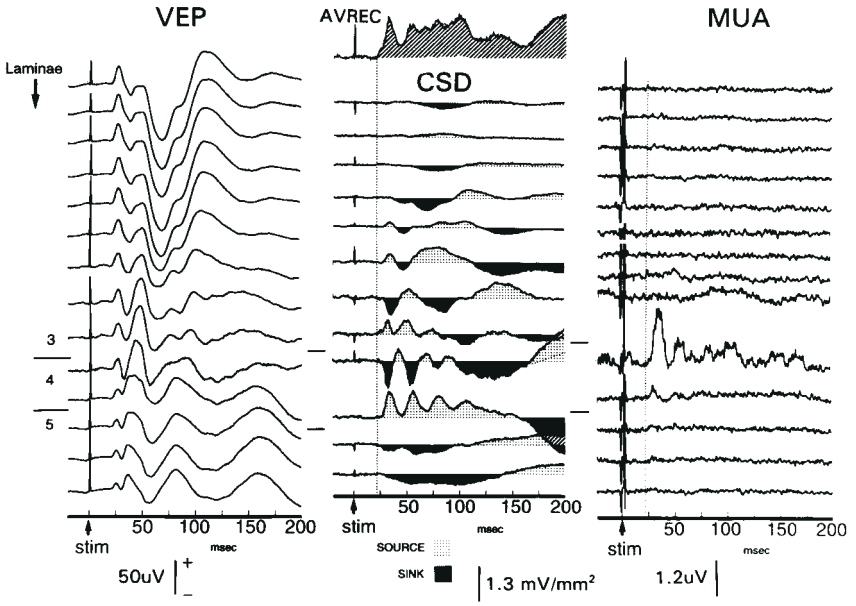

Figure 8. A laminar activity profile from the lateral bank of the IP sulcus, using a multielectrode with intercontact spacings of 150 mm. The profile was recorded from an electrode position 2.5 mm deeper than that which yielded the profile in Figure 7. Conventions are the same as in Figure 3.

field potential distribution that volume conducts out from the active region with a relatively linear fall-off. (ii) The second spatial derivative approximation of the CSD analysis identifies the locations of transmembrane current flow. As reviewed by Mitzdorf (1985), the current flow results primarily from synaptic activation of cortical tissue, white matter areas having basically flat CSD profiles, with occasional low-amplitude contamination from action potentials occurring near a recording electrode. Active white matter regions can be characterized, therefore, by multiunit activity in the presence of a near-zero second derivative. The grey/white matter boundary is thus obvious in most cases as the location at which the low-frequency components of the CSD drop to near-zero, though multiunit activity often extends considerably beyond this point (see e.g. Schroeder *et al.*, 1995). (iii) Appropriately bracketing the large components of the CSD profile provides a simple way to straddle an 'active' cortical region with a recording array. Application of these methods to subcortical visual structures was illustrated in detail earlier (Schroeder *et al.*, 1992).

The qualities of diffuse light stimulation in relation to the intent of the present study were evaluated in three empirical tests. First, the degree to which the stimulus reliably excites the

more peripheral retinal representations was determined by recording directly within these areas as described immediately above, and without changing the animal's fixation pattern (see Fig. 4*A*,*B*). Retinal eccentricity increases with depth (see Daniel and Whitteridge, 1961). Thus, recording from successive belts assesses the response over sizable steps in retinal eccentricity. Figure 4*C* depicts condensed CSD (AVREC) representations derived from a series of electrode positions along two penetrations through the medial/posterior operculum into the underlying peripheral representations in V1. The AVREC waveforms show that response amplitude is maintained over increasing retinal eccentricity (depth) in each of the penetrations. Latency, if anything, decreases with increase in retinal eccentricity. Decrease in amplitude and increase in latency would be expected if there were a dramatic fall-off in the intensity of stimulation over the more eccentric retinal regions. As a second evaluation of the quality of diffuse light stimulation, we sought to determine the extent to which the light scatter produced by the diffuser effectively stimulates peripheral portions of the retina. The data in Figure 4 suggest effective stimulation of 'near-peripheral' retinal locations. To follow up on this, we examined the sensitivity of flash-evoked responses (amplitude and onset latency) to systematic variations in eye position at one V1 recording site by recording light-evoked responses while the animal fixated: (i) in the center of the stimulus, (ii) at 4°, (iii) at 10°, (iv) at 16°, (v) at 23° and (vi) at 32° (the limit of our tracking system) lateral to the center of the stimulus (diffuser). Lamina 4C response latencies for the different eccentricities of stimulation were recorded in random order. These ranged from 26 to 29 ms, but did not vary systematically as a function of eccentricity. This indicates that the stimulation used here maintains sufficient intensity over the peripheral visual field out to >30° eccentric, such that no luminance decrement-induced latency increase can be detected. As a third evaluation of the quality of diffuse light stimulation, we compared flash-evoked laminar activity profiles with patterned flash and pattern reversal profiles obtained in the same recording site. This was done during penetrations in both V1 and V2. Patterned flash and pattern reversal data were collected with the animal performing a central fixation task (see Materials and Methods). Flash-evoked profiles were collected under the typical conditions of this study, with eye position unconstrained. In all cases, stimulus variations were presented at 2 Hz. Figure 5 displays laminar CSD profiles from one electrode position in V2, elicited by flash stimulation (left), patterned flash (middle) and pattern reversal (right). The most important point to note is that diffuse light produces activation of V1 and V2 that is comparable in quality to that produced by the stronger of the pattern stimuli (patterned flash). The responses produced by all stimuli have the same feedforward activation sequence, but differ in response timing, amplitude and laminar response amplitude distribution. The V1 findings (not displayed) are in precise agreement and are a direct replication of earlier findings from our laboratory (Schroeder *et al.*, 1991). The initial portions of flash and pattern/flash responses are remarkably similar, in that the first prominent sink begins at the depth of Lamina 4 (or 4C), and is followed by responses in the extragranular laminae. The initial response to flash is larger, due to the higher intensity and sharper rise time of the stimulus. Approximately 15 ms after response onset, the sink/source patterns elicited by diffuse flash and the patterned stimuli begin to diverge in several locations, e.g. in the infragranular laminae of V2. Somewhat larger differences between diffuse light and patterned-evoked responses are apparent after 75 ms latency in the extragranular laminae.

In sum, diffuse light produces robust responses in the foveal and immediate parafoveal representations in V1 and there is a clear correspondence between postsynaptic potential and action potential indices (CSD and MUA respectively) of local activation. Further, due to the intensity and the degree of light scatter, diffuse light produces high-intensity stimulation over large portions of the peripheral visual field, extending out to at least 30° eccentricity. Finally, laminar activation profiles in V1 and V2, whether in response to diffuse light, pattern flash or pattern reversal, have excitatory feedforward characteristics, with initial, excitatory response in and near Lamina 4, followed by responses in the extragranular laminae.

2. Laminar Activation Patterns in the Dorsal Pathway

Figure 6 depicts laminar activity profiles sampled from the ventral bank in the posterior STS (STSpv). STSpv is the region of the ventral bank of STS extending posteriorly from the STS/lateral sulcus junction, which contains MT and the immediately surrounding visual areas. Several points outlined for the V1 and V2 profiles merit review here. First, the local field potential profile (VEP, left) shows a region of maximal voltage gradient in the middle laminae, with a relatively linear fall-off (second derivative approaching zero) at the upper and lower boundaries of the tissue. Most of the superficial layer VEP components undergo polarity inversion within the region straddled by the electrode array. Second, the second-derivative approximation (CSD analysis) detects net local transmembrane current flow in the laminae where sharp changes in voltage gradient and inversions are observed. Finally, the pattern of net current sources and sinks thus resolved, in conjunction with the local action potential profile (MUA, right) outlines an excitatory feedforward activation pattern. Initial excitation occurs at the depth of Lamina 4, and this is followed by responses in the extragranular laminae. The activation profile in STSpv is thus similar to that in V1, although the initial response is sharper and larger than that in V1 and V2. The same is true for the other dorsal stream areas (below). The local contribution of STSpv to the late (post 85 ms) components of the VEP profile appears greater than that of V1. The laminar voltage gradients of the negative and positive components peaking at ~80 and 125 ms respectively, are sufficiently sharp that each exhibits a clear intracortical polarity inversion, underlain by sink/source and source/sink CSD configurations respectively. This contrasts with the relatively gentle voltage gradients and relatively low-amplitude CSD profile associated with the late components in V1.

Figures 7 and 8 depict laminar activity profiles recorded from the medial and lateral banks of the IP sulcus respectively. As in STSpv, there is a robust excitatory response to diffuse light and a feedforward laminar pattern. Initial excitation begins at the depth of Lamina 4 and is followed by activation of the extragranular laminae. Also as in STSpv, the laminar voltage gradient and associated CSD profile for late (post 85 ms) ERP components is greater than that in V1.

3. Laminar Activation Patterns in the Ventral Pathway

Figure 9 displays a laminar activity profile recorded from V4. The V4 data in the present report are a replication of an extensive V4 study by Givre *et al.* (1994). Several major findings are elaborated here because of they outline points of significant contrast between the response profiles of ventral stream areas

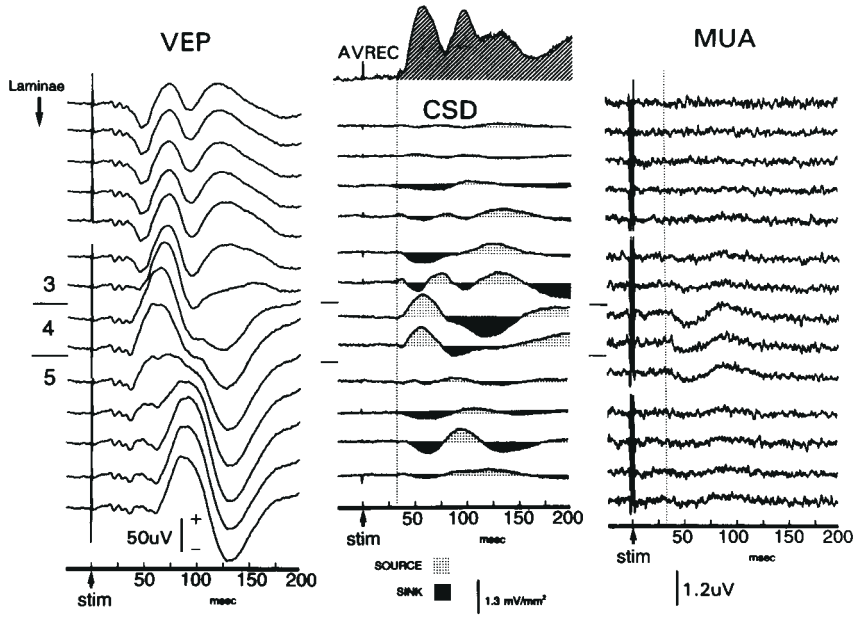

Figure 9. A laminar activity profile from V4 using a multielectrode with intercontact spacings of 150 mm. Conventions are the same as in Figure 3.

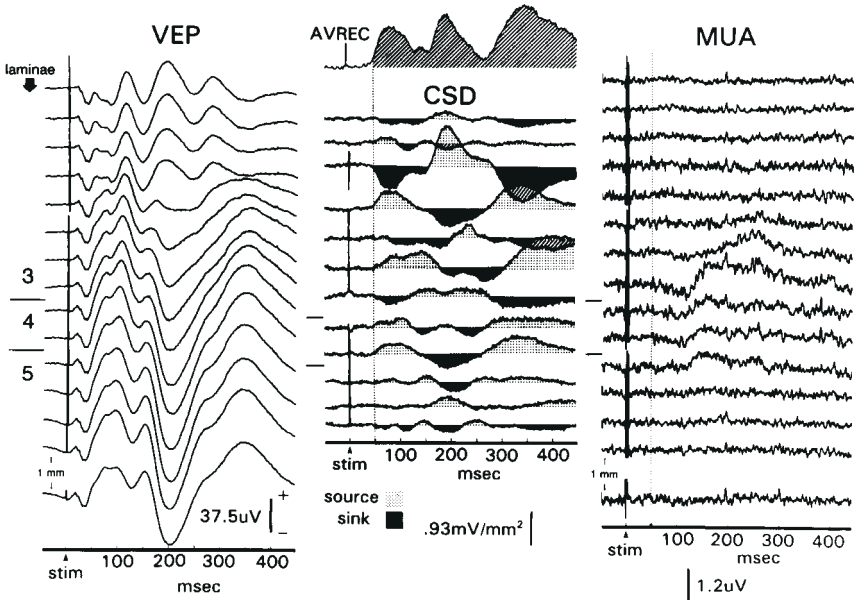

Figure 10. A laminar activity profile from IT using a multielectrode with intercontact spacings of 150 mm. Conventions are the same as in Figure 3.

and those described above. Specifically the profile in Figure 9 contrasts in two important ways with those recorded in lower pathway (V1/V2) and dorsal stream areas, and these apply to IT profiles as well (below). First, the initial response often consists of inhibition rather than excitation (see also Givre *et al.*, 1994). This is evident in the fact that the dominant early CSD component is a current source, associated with a depression in multiunit activity. This configuration reflects a net hyperpolarization of the local neuronal population. The current sinks above and below represent current return for circuit completion. Further, based on alignment of recordings with layers using both lesions and depth relative to the pial surface, Givre *et al.* (1994) determined that the laminar activation pattern in V4 is different from that in the lower visual areas. That is, the initial response in V4 lacks a clear mid-lamina focus, but rather begins in multiple laminae simultaneously. This contrasts with the 'ascending' pattern of starting in Lamina 4 and then spreading to the upper and lower laminae. In the case of Figure 9, for example, the response in the superficial laminae is, if anything, earlier than that in lower laminae. This is best appreciated by contrast with the laminar activation in dorsal stream area STSpv (Fig. 6). Thus, the best descriptor of the laminar activation pattern in V4 is 'multilaminar, or columnar', using the terminology of Felleman and Van Essen (1991). These two sets of observations, in conjunction with response latency data, were interpreted by Givre *et al.* (1994) to mean that the initial response in V4 reflects

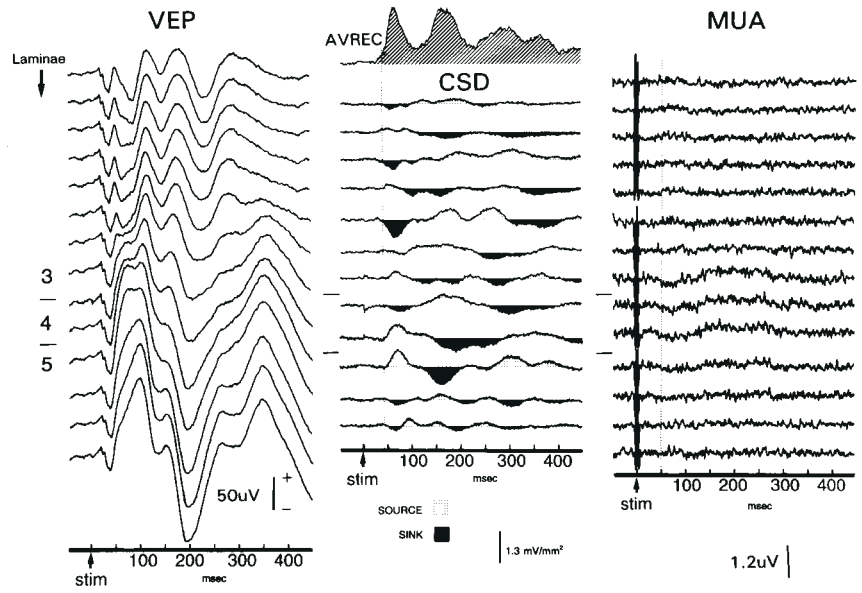

Figure 11. A laminar activity profile from IT using a multielectrode with intercontact spacings of 150 mm. Conventions are the same as in Figure 3.

a 'modulatory' input, as opposed to an excitatory feedforward input. The ascending excitatory input is believed to be manifested in the later current sink and associated multiunit discharge in the location corresponding to Lamina 4. Finally, as for the other extrastriate areas, V4 data suggest a more prominent local contribution to the late VEP components than that from V1 (see also Givre *et al.*, 1994). All of the later (post 85 ms) components undergo intracortical polarity inversion in V4.

Figures 10 and 11 display laminar activity profiles recorded in ventral stream area IT. The two points of contrast with lower pathway and dorsal stream areas, that were outlined above for V4, also pertain to IT. Although less clearly so than in V4, the initial response appears to consist of net inhibition rather than net excitation. In both Figures 10 and 11, for example, the shortest latency CSD components are associated with MUA depression centered at, and slightly above, the depth of Lamina 4. This CSD/MUA configuration most likely reflects a net local hyperpolarization; the current sinks represent current return for circuit closure, rather than sites of ligand-gated transmembrane current flow. The same appears to be the case for the initial response epoch in Figure 11. It is possible also that the response onset in the uppermost portions of these CSD profiles, which are without MUA correlates, reflects an altogether separate set of inhibitory and/or excitatory cellular processes. In this case, the net response would appear to reflect PSPs insufficient to cross action potential thresholds in local neurons. On occasion, the initial response in IT is seen as a configuration of clear, phasic CSD components with no discernable correlate in the multiunit activity profile, which fits with such a 'subthreshold' interpretation. In any case, the onset of response in IT profile lacks a clear mid-lamina focus. As in V4, there is no timing offset between the response onset in the middle versus the upper or lower laminae. Thus, the best descriptor of the laminar activation pattern in IT is 'multilaminar/columnar', rather than feedforward. Although the first (50–100 ms) epoch of the IT response profile is reliable, later portions of the response are more variable (e.g. the post 100 ms response in Fig. 10 versus Fig. 11). The increased multiunit activity occurring at ~100–125 ms (see Fig. 10, right column, middle) may reflect the excitatory

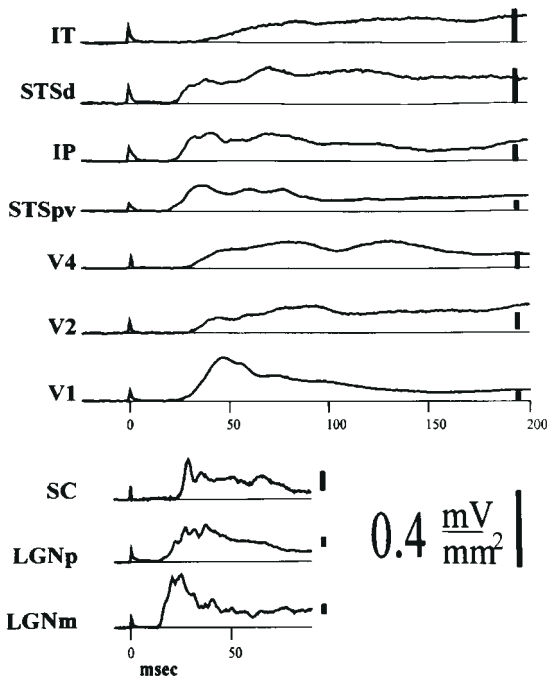

Figure 12. Grand mean AVREC waveforms for each visual area. These were obtained by averaging across penetrations and animals, with penetration as the unit of observation. Only the first 200 ms poststimulus is shown, although activity in many areas continues past this point. All of the response waveforms scored for the onset latency analyses described in the text (see also Fig.13) are included in the appropriate grand mean waveform. Number of subjects/observations upon which each waveform is based are: LGNm 3/4, LGNp 3/5, SC 1/4, V1 6/63, V2 4/21, V4 5/29, STSpv 4/13, IP 4/16, STSd 5/33, IT 5/35.

feedforward input mediated by ascending projections from lower areas of the ventral stream because, as predicted on anatomical grounds (Rockland and Pandya, 1979), it is most prominent at and immediately above the location of Lamina 4. Finally, as in the other extrastriate areas, IT has a more prominent local contribution to the later VEP components than

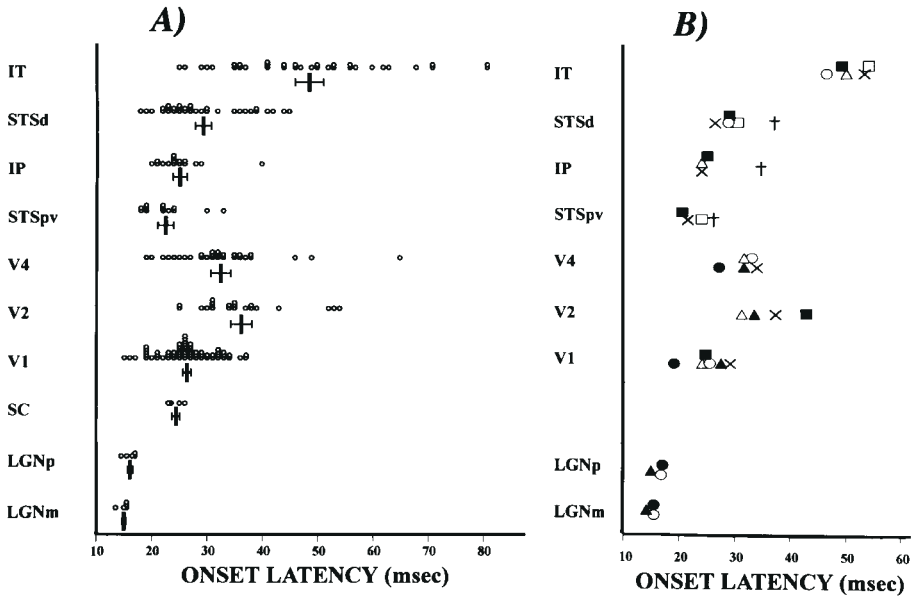

Figure 13. (*A*) Scatter plots of onset latencies, organized by visual area, including the mean and standard error of the distribution for each for each area. Values represent onset latency, as determined with statistically based scoring, as described in methods. Each entry indicates one onset latency, scored for one electrode penetration. (*B*) Individual subject mean latencies for each area. No entry is made for the superior colliculus (SC) since the SC latency distribution was sampled from one subject.

that of V1. While there does appear to be local contribution to a surface negative VEP component peaking at ~80 ms latency, the most obvious contributions are to a series of positive/negative deflections occurring between 200 and 300 ms latency and to a late negative component that peaks between 350 and 450 ms latency. For most of the later VEP components, the laminar voltage gradient is sufficiently sharp that an obvious polarity inversion occurs across the local laminar expanse.

3. Temporal Activation Patterns in the Visual Pathways: To get an overall impression of the 'typical' temporal activity pattern within the individual visual areas comprising the system, we computed grand mean AVREC waveforms for the first 200 ms of poststimulus time for each area (Fig. 12). These waveforms show that a single 10 μsec light pulse produces transmembrane current flow beginning at ~15 ms poststimulus (response onset in LGN) and lasting to well beyond the frame of this analysis (200 ms) in the higher visual areas. They also outline characteristic differences between temporal activity profiles in the different components of the system. The mean AVREC for magnocellular LGN, relative to that for parvocellular LGN, shows an earlier onset, a sharper onset and higher peak amplitude, but a less prominent sustained activity component. The superior colli -culus AVREC indicates a sharp onset that is later than that for either division of LGN. Relative to those of the higher cortical areas, the V1 AVREC shows a predominance of early (pre-75 ms) activity. The V2 AVREC begins later than that for V1 and is clearly dominated by later (post-75 ms) activity. The V4 AVREC has no onset latency lag relative to that of V2, but is similarly dominated by later activity. The temporal pattern of activity in IT is similar to that in V4, albeit with a later onset and longer duration. Comparisons within levels, for example between V4 and STSpv, reveal that the activity of dorsal stream areas has sharper onset and rise time and begins earlier than that of ventral stream areas.

In order to describe more clearly the temporal activation pattern across the structures comprising the dorsal and ventral pathways, Figure 13*A* displays the onset latency distributions for

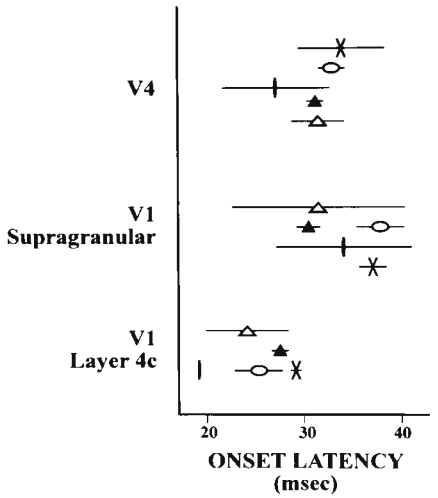

Figure 14. Individual subject mean onset latencies and standard deviations for the thalamorecipient (4C) and supragranular laminae of V1 and for the initial response in any lamina of V4. Included in this figure are all data from each of the four subjects with data in both V1 and V4.

each of the visual areas in this study, grouped across subjects. To address individual subject variations, Figure 13*B* displays the mean latencies for each area, computed on a within-subject basis. In the subjects with a sufficiently wide sample, the overall latency pattern across areas, characteristic of the grouped data, is clearly evident.

Certain temporal comparisons are motivated by earlier work. First, CSD measures in LGN show a latency difference between parvocellular (P) and magnocellular (M) laminae consistent with our earlier findings based on multiunit activity, in a much larger sample (Schroeder *et al.*, 1989). Secondly, at several cortical levels there is a consistent latency advantage for the dorsal over the ventral stream. Mean latency in STSpv is significantly shorter

(10.0 ms, $P < 0.05$) than the corresponding value in V4 and mean latency in IP is 23.4 ms shorter ($P < 0.05$) than that in IT. The mean latency difference between STSd and IT appears substantial (19.8 ms), but is not statistically significant ($P < 0.07$). A third expected result is that there are predictable and significant ($P < 0.05$) time lags across many points in the system such as: (i) from LGN to V1 (10.9 ms), (ii) from V1 to V2 (9.8 ms), and (iii) from STSpv to STSd (7.1 ms). Most of these differences are seen on a within-animal basis. The difference between LGN and V1 latencies, for example, is significant ($P < 0.05$) in each of the three animals with both LGN and V1 data. The last set of observations is consistent with serial organization, as deduced from system connectivity models presented by a number of groups (see recent reviews by Maunsell, 1995; Ungerleider, 1995).

Finally, comparison of V1 latencies with those in higher-order cortices reveals the following. Consistent with earlier findings by Givre *et al.* (1994), the average onset latency in V4 (32.3 ms) is significantly earlier ($P < 0.05$) than the average latency in the supragranular laminae of V1 (35.5). Although, on a within-subject basis, this difference is significant for only one subject, we are not inclined to regard it as an artifact of comparison across animals because the trend is evident in each one of the subjects (Fig. 14). This result does not stem from comparison of latencies across different retinal eccentricities in V1 and V4. In one animal, comparison was made between opercular V1 recordings representing foveal/parafoveal space (Dow *et al.*, 1985) and deep tissues of V1, representing extrafoveal visual space (Daniel and Whitteridge, 1961). The average latency of foveal/parafoveal responses was 26.4 ms (SD = 5.1) and for peripheral responses it was 19.3 ms (SD = 2.9). This gain of ~7 ms is not enough to overcome the 9–15 ms latency lag between the granular and supragranular laminae of V1 (Maunsell and Gibson, 1992; Givre *et al.*, 1994; present results). While the nonsignificant comparisons must be interpreted cautiously, it is safe to state that our data do not support the position that initial activity in V4 is driven through the major ascending pathway (supragranular V1 to V2 to V4). A somewhat similar situation is found in examining the latencies of visual areas in the posterior superior temporal sulcus. The average latency in STSpv (mean = 20.3 ms, SD = 1.5) is significantly earlier ($P < 0.05$) than that in Lamina 4C of foveal V1 (V1f: mean = 27.9ms, SD = 3.5). This difference between STSpv and V1f is significant ($p < 0.05$) on a within-animal basis, but only two of our subjects yielded data from both areas, and data from one of these animals indicated that STSpv latencies are not significantly different ($P > 0.05$) from those in the extreme peripheral representation of V1 (V1p: mean = 20.4, SD = 2.7).

Discussion

Intracortical Laminar Activation Profiles

There have been relatively few studies of cortical laminar activation profiles in the visual system, and these were confined to areas V1, V2 and V4. The excitatory feedforward pattern we have observed in V1 and V2 is entirely consistent with earlier reports (Mitzdorf and Singer, 1979; Kraut *et al.*, 1985, Schroeder *et al.*, 1990a,b, 1991, 1997a; Givre *et al.*, 1994, 1995), as is the relative invariance of this pattern over different forms of stimulation (Mitzdorf, 1986; Schroeder *et al.*, 1991). The basic activation pattern we observed in V1 and V2 entails initial excitation at a depth corresponding to Lamina 4 followed activation of the supra and infragranular laminae. The present study found a similar activation profile in dorsal stream visual areas, in that the initial excitation was reliably observed in and near Lamina 4. The degree of spatial (laminar) variation we observe in this pattern depends on both the degree of resolution imposed by a chosen intercontact spacing on the electrode array and the degree of underlying anatomic variation (e.g. Rockland and Pandya, 1979; Felleman and Van Essen, 1991; Rockland, 1997).

In agreement with earlier reports (Mitzdorf, 1985, 1986; Schroeder *et al.*, 1991; Givre *et al.*, 1995), variations in stimulation parameters were observed to alter the timing and laminar distribution of responses, but not the basic activation sequence. The activation sequence in V1 is sufficiently robust that it persists in the context of paroxysmal activation, triggered by disinhibition (Schroeder *et al.*, 1997a). The laminar activation pattern found in V1 and V2 and in dorsal stream visual areas is like that found in auditory (Mueller-Preuss and Mitzdorf, 1984; Steinschneider *et al.*, 1992) and somatosensory cortices (Kulics and Cauller, 1986; Schroeder *et al.*, 1995, 1997b) and this is the pattern predicted by the anatomy of ascending projection patterns (Rockland and Pandya, 1979). Despite the wide objections, on both anatomical and physiological bases, to the concept of a strict, visual hierarchy (reviewed in Rockland, 1997), it is generally conceded that ascending or feedforward inputs have their most dense terminations in and near Lamina 4 of the target area. This is the key to setting up the excitatory feedforward activation pattern that we describe. The degree of variation in the laminar activation pattern across areas clearly merits further investigation; however, the regularity of the initial excitation in the middle laminae remains striking, particularly when contrasted with our findings in ventral stream areas V4 and IT (see also Givre *et al.*, 1994).

Both V4 and IT exhibit a laminar activation profile best characterized as multilaminar/columnar, in that initial responses are distributed across the laminae, rather than concentrated at the depth of Lamina 4. Moreover, the combined measures of CSD and multiunit activity indicate a predominance of initial PSPs which are associated with either no change, or a suppression of action potentials. The first prominent excitation appears subsequent to this at a depth corresponding to Lamina 4. Collectively, these observations suggest that in the ventral stream, the initial portion of the response to diffuse light reflects a stimulus-evoked modulation of local excitability, rather than excitation. It should be emphasized that this interesting activation pattern may be specific to stimuli that contain a large luminance component. Further studies will be necessary to determine if this is the case.

Possible sources of the initial 'modulatory' inputs to V4 include direct projections from pulvinar (Benevento and Rezak, 1976; Ogren and Hendrickson, 1977; Lysakowski *et al.*, 1988; Tanaka *et al.*, 1990) and koniocellular LGN neurons (Benevento and Yoshida, 1981; Fries, 1981; Lysakowski *et al.*, 1988; Yoshida and Benevento, 1981; Yukie *et al.*, 1979; Yukie and Iwai, 1981; Tanaka *et al.*, 1990). However, available evidence (see e.g. Hendry, and Yoshioka, 1994) suggests that the latter have slowly conducting axons, and are thus unlikely to drive the short latency activity in V4. Similarly, direct input from pulvinar (Iwai and Mishkin, 1964; Benevento and Rezak, 1976) could drive initial 'modulation' in IT. Neither the laminar patterns of koniocellular LGN projections to extrastriate cortex, nor those of pulvinar-extrastriate projections (see e.g. Benevento and Rezak, 1976; Benevento and Yoshida, 1981) provide a clear match to the multilaminar/columnar activation profiles we observe in V4 and

IT, although some of the latter do have a 'quasi-columnar' termination pattern (K.S. Rockland, personal communication; see Saleem *et al.*, 1993).

An alternative possibility is that lateral corticocortical connections provide initial inputs to the structures in the ventral stream. In current models (Felleman and Van Essen, 1991; Ungerleider, 1995), MT is placed at the same hierarchical level as V4 and several dorsal stream areas in the IP sulcus and STS are placed at levels corresponding to the divisions of IT. The multilaminar/columnar activation profile, while atypical for thalamic and ascending cortical inputs, is actually predicted by the anatomy of 'lateral' projections, such as between MT and V4 (see Felleman and Van Essen, 1991). As discussed below, our timing data are consistent with driving of the early activity in V4 by fast lateral inputs from STSpv, which includes area MT (see also Ferrera *et al.*, 1994), and similarly with the possibility that initial activity in IT is driven by lateral inputs from the upper bank of STS or from the regions in the IP sulcus. The notion of parietotemporal modulation is consistent with both dorsal/ventral stream cross-connections and mixing of P and M properties in the higher cortical visual areas (see Merrigan and Maunsell, 1993; Maunsell, 1995). The apparent asymmetry of this mixing in favor of the M system (e.g. Maunsell *et al.*, 1990) may reflect anatomical asymmetry or preferential expression due to the greater speed of M inputs (see below). This issue requires additional experimentation.

A Cross-regional Temporal Activation Profile

Systematic evaluation of response latencies across the structures of the visual pathways provides information along two lines. First, we confirm a large dorsal/ventral stream latency advantage in a large sample obtained from awake monkeys, and we place clear dimensions on this advantage. STSpv activity begins at 22.3 ms, relative to ~32.3 ms in V4, and the same comparison for IP and IT yields 25.8 and 49.2 ms respectively. The generality of our findings is supported by the fact that the dorsal/ventral stream latency advantage is observed across a number of laboratories, using a variety of stimulation and recording methods (reviewed by Nowak and Bullier, 1997). Considering that in both V4 and IT, the 'excitatory-feedforward' response latency (indexed by combined action potential and CSD measures) is greater than initial PSP onset latency (as indexed by the CSD – see also Givre *et al.*, 1994), the dorsal/ventral speed advantage for excitatory feedforward responses may be even larger than that estimated by unadjusted CSD latencies. However, there are certain conditions, e.g. isoluminant stimulation, under which the dorsal/ventral stream latency advantage may be predicted to reduce, disappear or even reverse, and these will be important targets of further study. Second, while the overall latency pattern across the system is generally consistent with a serial model of processing, there is at least one exception. The average latency of the initial 'modulatory' activity in V4 is significantly earlier than that in the supragranular laminae of V1, the origin of the major ascending afferents from V1. Several reports (Robinson and Rugg, 1988; Vogels and Orban, 1991; Celebrini *et al.*, 1993; Nowak and Bullier, 1995; Bullier and Nowak, 1995) cited V1 latencies with much longer mean values and wider ranges than ours, due mainly to the choice of stimuli and/or to the study of anesthetized animals. Our V1 latency data (mean 26.3 ms, range 18–37 ms) align very well with those from recent experiments conducted in unanesthetized monkeys (Maunsell and Gibson, 1992), whose Lamina 4 latencies range from 20 to 31 ms. Moreover, both groups (Maunsell and Gibson, 1992; Givre *et al.*, 1994; present report), and Bullier and Nowak (1995), find a substantial (9–15 ms) lag between responses in the thalamo-recipient and supragranular laminae of V1.

Our V4 data appear at first to conflict with those of Maunsell and colleagues. Based on transmembrane current flow (CSD) latencies, we find that the initial response in V4 is significantly earlier than that in supragranular V1. Based on action potential recordings, Maunsell (1987) describes a V1 to V4 latency difference of ~22 ms, which is compatible with serial feed-forward activation via the upper laminae of V1. However, action potential latencies index only the onset of excitatory postsynaptic responses of a 'suprathreshold' character and CSD measures reveal that the initial response in V4 is net local hyperpolarization, whose action potential correlate is a subtle decrease in activity (present results; Givre *et al.*, 1994). Givre *et al.* (1994) also observed a subsequent increase in action potentials at ~50 ms, which corresponds to the latency reported by Maunsell (1987). Thus, the transmembrane current flow latency appears to index an initial modulatory input, while action potential latency reflects a later corticocortical activation, predicted by a serial model of striate-to-extrastriate activation (e.g. Felleman and Van Essen, 1991). A similar reasoning may explain why our average CSD latency of 49.2 in IT is shorter than earlier reports of 60–120 ms for action potential latencies (Ashford and Fuster, 1985; Richmond *et al.*, 1987; Oram and Perrett, 1992).

Our V1-STSpv (MT) latency comparison is consistent with that of Raiguel *et al.* (1989), in that we find shorter average latencies in the latter structure. We also found that the latencies in the peripheral retinal representation of V1 are the shortest subset of V1 latencies, and in fact are shorter than those in STSpv. This suggests a possible route by which STSpv could be activated through V1, without recourse to a subcortical mechanism that bypasses V1. However, both our findings and those of Raiguel *et al.* (1989) conflict with the 11 ms lag in MT relative to V1 reported by Maunsell (1987). While the discrepancy between the present results and Maunsell's V4 data has a potential explanation (see above), this explanation would not hold for the initial response in STSpv, which appears to reflect excitatory feedforward activation.

Implications for Human Research

The temporal activity patterns evident in the grand mean AVREC waveforms have direct implications for understanding how noninvasive event-related electro- and magneto-encephalographic measures (ERP and MEG) index visual pathway activity in humans. The small latency differences across the system combined with the long response durations (see Fig. 12) make it likely that multiple structures contribute to any surface ERP or MEG component. Despite this, it appears clear that any contribution from V1 is likely to be limited to early (pre-150 ms) ERP and MEG components. Early components not originating in V1 are most likely to arise from dorsal stream areas. Further dissection of the contributions from various visual pathway areas appears possible through the manipulation of their differential stimulus and task sensitivities (see e.g. Foxe *et al.*, 1994).

Violations of Serial Order and the Hierarchy

Several aspects of our findings conflict with proposed patterns of serial connectivity. Most notable is the lack of clear latency offset between the initial cortical stage in V1 and higher-order area V4. Serial projection from V1 to V4 requires that responses in V4 follow those in the supragranular laminae of V1 (the origin

of the major ascending pathways to V2 and V4). However, despite common assumptions to the contrary, strict serial organization is not a requirement for a hierarchy (Van Essen *et al.*, 1992). Direct subcortical to extrastriate projections, 'level jumping' and lateral connections within the intracortical pathways (e.g. Felleman and Van Essen, 1991), as well as both latency data (present results; Raiguel *et al.*, 1989; Bullier and Nowak, 1995; see review by Nowak *et al.*, 1997) and laminar patterns of initial activation in V4 and IT all appear to argue against a simple serial model. Nonetheless, ascension of the visual hierarchy is associated with progressions of physiological properties (Maunsell and Newsome, 1987) that most likely result from feedforward (serial) convergence. A fact that may reconcile the functional hierarchy with the lack of strict serial connectivity is that processing in any location appears to be based on numerous temporal components or 'waves' of activity (see also Nowak and Bullier, 1997). In V4, there appear to be at least two early activity components – an initial input that bypasses supragranular V1, followed by an excitatory feedforward input presumably relayed through supragranular V1. A similar situation is apparent in IT. Distinguishing the input routes and origins of different activity components may be important in understanding the temporal dynamics of processing within any one location (e.g. Richmond *et al.*, 1987). It is noteworthy that finding separable temporal processing components within a location is exactly what one would expect if inputs from a common source (the eye) travel over several heterogeneous pathways and converge on a common location.

Functional Significance of the Temporal Activation Profile

In contrast to recent analyses focusing on information encoding in the temporal spike patterns of neurons (e.g. Richmond *et al.*, 1987; Shadlen and Newsome, 1994; McClurkin *et al.*, 1996; Victor and Purpura, 1996) or on the role of correlated activity in binding and related phenomena (e.g. Eckhorn *et al.*, 1988; Gray and Singer, 1989; Bressler, 1995, 1996; Gawne *et al.*, 1996), our studies address the spatiotemporal structure of brain responses to visual input. One consequence of the dorsal–ventral stream speed advantage is that it supports a temporal ordering of dorsal stream- versus ventral stream-mediated components of visual discriminative function, such as grouping/figure–ground segregation versus object recognition. Another consequence of the speed advantage, alluded to above, is that it sets up an interactive mode of processing in which initial stimulus-evoked activity at each stage of the ventral stream can be modulated by a fast input, elicited by the same stimulus, and conveyed by lateral projections from the dorsal stream. This could be important in diverse functions such as promoting figure–ground segregation for moving objects and elicitation of a subject's attention by such objects. These issues merit further experimentation. A particular challenge for future studies will be to relate the temporal patterns of processing in a given cortical area to the spatiotemporal structure of activity across the system as a whole.

Notes

We thank Drs D.C. Javitt, J.C. Arezzo and H.G. Vaughan, Jr for advice and support, Robert Lindsley, Shirley Seto, Mona Litwak and Chester Freeman for technical assistance, Dr George Lantos for valuable assistance in MR imaging and May Huang, Robert Lindsley and Dr S.U. Walkley for histology. We also thank Drs Kathleen S. Rockland and Anna W. Roe for helpful discussions and comments on earlier versions of the manuscript. Supported by MH47939, MH55620, T32GM7288-NIGMS and by the Human Frontier Science Project.

Address correspondence to C.E. Schroeder, Program in Cognitive Neuroscience and Schizophrenia, Nathan Kline Institute for Psychiatric Research, 140 Old Orangeburg Road, Orangeburg, NY 10962, USA. Email: schrod@nki.rfmh.org.

References

Allison T, McCarthy G, Nobre A, Puce A, Belger A (1994) Human extrastriate visual cortex and the perception of faces, words, numbers and colors. Cereb Cortex 4:544–554.

Ashford JW, Fuster JM (1985) Occipital and inferotemporal responses to visual signals in the monkey. Exp Neurol 90:444–466.

Benevento LA, Rezak M (1976) The cortical projections of the inferior pulvinar and the adjacent lateral pulvinar in the rhesus monkey (*Macaca mulatta*). Brain Res 108:1–24.

Benevento LA, Yoshida K (1981) The afferent and efferent organization of the lateral geniculo-prestriate pathway in the macaque monkey. J Comp Neurol 203: 455–474.

Best J, Reuss S, Dinse HRO (1986) Lamina-specific latencies following photic stimulation in the cat striate cortex. Brain Res 385:356–360.

Bressler SL (1995) Large scale cortical networks and cognition. Brain Res Rev 20: 288–304.

Bressler SL (1996) Interareal synchronization in visual cortex. Behav Brain Res 76: 37–49.

Bullier J, Nowak LG (1995) Parallel versus serial processing: new vistas on the distributed organization of the visual system. Curr Opin Neurobiol 5:497–503.

Celebrini S, Thorpe S, Trotter Y, Imbert M (1993) Dynamics of orientation coding in area V1 of the awake primate. Vis Neurosci 10:811–825.

Connors B (1984) Initiation of synchronized bursting in neocortex. Nature 310:685–687.

Daniel PM, Whitteridge D (1961) The representation of the visual field on the cerebral cortex in monkeys. J Physiol 159:203–221.

Daniel WW (1978) Applied nonparametric statistics. Boston, MA: Houghton-Mifflin.

Donders FC (1968) On the speed of mental processes; translation in Acta Psychol 30, Attention and Performance 11 (Koster, WG, ed.), pp. 412–431 (1969).

Dow BM, Vautin RG, Bauer R (1985) Mapping of visual space onto foveal striate cortex in the macaque monkey. J Neurosci 5:890–902.

Eckhorn R, Bauer W, Jordan W, Brosch M, Kruse W, Munk M, Reitboek H (1988) Coherent oscillations: a mechanism of feature linking in the visual cortex? Biol Cybern 60:121–130.

Felleman DJ, Van Essen DC (1991) Distributed hierarchical processing in the primate cerebral cortex. Cereb Cortex 1:1–47.

Ferrera VP, Nealey TA, Maunsell JHR (1994) Responses in Macaque visual area V4 following inactivation of the parvo and magno LGN pathways. J Neurosci 14:2080–2088.

Foxe JJ, Mehta AD, Ulbert I, Simpson GV, Vaughan HG Jr, Ritter W, Schroeder MM, Schroeder CE (1994) Integration of human and monkey electrophysiology in the study of sensory processing and attention. Soc Neurosci Abstr 20:576.

Freeman JA, Nicholson C (1975) Experimental optimization of current source density technique for anuran cerebellum. J Neurophysiol 38:369–382.

Fries W (1981) The projection from the lateral geniculate nucleus to the prestriate cortex of the macaque monkey. Proc R Soc Lond B 213:73–80.

Gawne TJ, Kjaer TW, Richmond BJ (1996) Latency: another potential code for feature binding in striate cortex. J Neurophysiol 76: 1356–1360.

Givre SJ, Schroeder CE, Arezzo J (1994) Contribution of extrastriate area V4 to the surface-recorded flash VEP in the awake macaque. Vis Res 34:415–438.

Givre SJ, Arezzo JC, Schroeder CE (1995) Effects of wavelength on the timing and laminar distribution of illuminance-evoked activity in macaque V1. Vis Neurosci 12:229–239.

Gray CM, Singer W (1989) Stimulus-specific neuronal oscillations in orientation columns of cat visual cortex. Proc Natl Acad Sci USA 86:1698–1702.

Halgren E, Baudena P, Clarke JM, Heit G, Liegeois C, Chauvel P, Musolino A (1994) Intracerebral potentials to rare target and distractor auditory and visual stimuli I. Superior temporal plane and parietal lobe. Electroenceph Clin Neurophysiol 94:191–220.

Hendry SHC, Yoshioka T (1994) A neurochemically distinct third channel

in the macaque dorsal lateral geniculate nucleus. Science 264:575–577.
Hendry SHC, J, deBlas AL and Jones EG (1990) Distribution and plasticity of immunocytochemically localized $GABA_A$ receptors in adult monkey visual cortex. J Neurosci 10:2438–2450.
Iwai E, Mishkin M (1964) Further evidence on the locus of the visual area in the temporal lobe of the monkey. Exp Neurol 25:585–594.
Jones EG (1990) Determinants of the cytoarchitecture of the cerebral cortex. In: Signal and sense: local and global order in perceptual maps (Edelman GM, Gall WE, Cowan WM eds), pp. 3–49. New York: Wiley Liss.
Kraut M, Arezzo J, Vaughan HG Jr (1985) Intracortical generators of the flash VEP in monkeys. Electroenceph Clin Neurophysiol 62:300–312.
Kulics AT, Cauller LJ (1986) Cerebral cortical somatosensory evoked responses, multiple unit activity and current source densities: their interrelationships and significance to somatic sensation as revealed by stimulation of the awake monkey's hand. Exp Brain Res 62:46–60.
Lamme VAF, van Dijk BW, Spekreijse H (1993) Contour from motion processing occurs in primary visual cortex. Nature 363:541–543.
Lysakowski A, Standage GP, Benevento LA (1998) An investigation of collateral projections of the LGN and other subcortical structures to cortical areas V1 and V4 in the macaque monkey: a double labeled retrograde tracer study. Exp Brain Res 69:651–661.
Maunsell JHR (1987) Physiological evidence of two visual subsystems. In: Matters of intelligence (Viana L, ed.), pp. 59–87. Dordrecht: Reidel.
Maunsell JHR (1995) The brain's visual world: representation of visual targets in cerebral cortex. Science 270:764–769.
Maunsell JHR, Newsome WT (1987) Visual processing in monkey extrastriate cortex. Annu Rev Neurosci 10:363–401.
Maunsell JHR, Gibson JR (1992) Visual response latencies in striate cortex of the macaque monkey. J. Neurophysiol. 68:1332–1344.
Maunsell JHR, Nealy TA, DePriest DD (1990) Magnocellular and parvocellular contributions to responses in the middle temporal visual area (MT) of the macaque monkey. J. Neurophysiol. 10:3323–3334.
Merrigan WH, Maunsell JHR (1993) How parallel are the primate visual pathways. Annu Rev Neurosci 16:369–402.
McClurkin JW, Gawne TJ, Optican LM, Richmond BJ (1991) Lateral geniculate neurons in behaving primates. II. Encoding of visual information in the temporal shape of the response. J Neurophysiol 66:794–808.
McClurkin JW, Optican LM (1996) Primate striate and prestriate cortical neurons during discrimination I: Simultaneous temporal encoding of information about color and pattern. J Neurophysiol 75:481–495.
McClurkin JW, Zarbock JA, Optican LM (1996) Primate striate and prestriate cortical neurons during discrimination II: Separable codes for color and pattern. J Neurophysiol 75:496–507.
Mitzdorf U (1985) Current source-density method and application in cat cerebral cortex: investigation of evoked potentials and EEG phenomena. Physiol Rev 65:37–100.
Mitzdorf U (1986) The physiological causes of the VEP: current source density analysis of electrically and visually evoked potentials. In: Evoked potentials (Cracco R, Bodis-Wollner I, eds), pp. 141–154. New York: Allan R. Liss.
Mitzdorf U, Singer W (1979) Excitatory synaptic ensemble properties in the visual cortex of the macaque monkey: a current source density analysis of electrically evoked potentials. J Comp Neurol 187:71–84.
Mueller-Preuss P, Mitzdorf U (1984) Functional anatomy of the inferior colliculus and auditory cortex: current source density analysis of click-evoked potentials. Hearing Res 16:133–142.
Munk MHJ, Nowak LG, Girard P, Chounlamountri N, Bullier J (1995) Visual latencies in cytochrome oxidase bands of macaque area V2. Proc Natl Acad Sci USA 92:988–992.
Nowak, LG, Bullier, J (1997) The timing of information transfer in the visual system. In: Cerebral cortex, vol. 12: Extrastriate cortex (Rockland KS, Kaas J, Peters A, eds), pp. 205–241. New York: Plenum Press.
Nowak LG, Munk MHJ, Girard P, Bullier J (1995) Visual latencies in areas V1 and V2 of the macaque monkey. Vis Neurosci 12:371–384.
Ogren MP, Hendrickson AE (1977) The distribution of pulvinar terminals in visual areas 17 and 18 of the monkey. Brain Res 137:343–350.
Optican LM, Richmond BJ (1987) Temporal encoding of two dimensional patterns by single units of primate inferior temporal cortex. J Neurophysiol 57:162–178.
Oram MW, Perrett DI (1992) Time course of neural responses discriminating different views of the face and head. J Neurophysiol, 68:70–84.
Raiguel SE, Lagae L, Gulyas B, Orban GA (1989) Response latencies of visual cells in macaque areas V1, V2 and V5. Brain Res 493:153–159.
Richmond BJ, Optican LM (1987) Temporal encoding of two dimensional patterns by single units in primate inferotemporal cortex II. Quantification of response waveforms. J Neurophysiol 57:147–161.
Richmond BJ, Optican LM, Podell M, Spitzer H (1987) Temporal encoding of two dimensional patterns by single units in primate inferior temporal cortex. I. Response characteristics. J Neurophysiol 57:132–146.
Robinson DL, Rugg MD (1988) Latencies of visually responsive neurons in various regions of the rhesus monkey brain and their relation to human visual responses. Biol Psychol 26:111–116.
Rockland KS (1997) Elements of cortical architecture: hierarchy revisited. In: Cerebral cortex, vol. 12: Extrastriate cortex(Rockland KS, Kaas J, Peters A, eds), pp. 243–293. New York: Plenum Press.
Rockland KS, Pandya DN (1979) Laminar origins and terminations of cortical connections in the occipital lobe in the rhesus monkey. Brain Res 179:3–20.
Saleem KS, Tanaka K, Rockland, KS (1993) Specific and columnar projections form area TEO to TE in the macaque inferotemporal cortex. Cereb Cortex 3:454–464.
Schroeder CE (1995) Defining the neural bases of visual selective attention: conceptual and empirical issues. Int J Neurosci 80:65–78.
Schroeder CE, Tenke CE, Arezzo JC, Vaughan HG Jr (1989) Timing and distribution of flash-evoked activity in the lateral geniculate nucleus of the alert monkey. Brain Res 477:183–195.
Schroeder CE, Tenke CE, Givre SJ, Arezzo JC, Vaughan HG Jr (1990a) Laminar analysis of bicuculline-induced epileptiform activity in Area 17 of the awake macaque. Brain Res 515:326–330.
Schroeder CE, Tenke CE, Givre SJ, Arezzo JC, Vaughan HG Jr (1990b) Binocularity in the lateral geniculate nucleus of the alert macaque. Brain Res 521:303–310.
Schroeder CE, Tenke CE, Givre SJ, Arezzo JC, Vaughan HG Jr (1991) Striate cortical contribution to the surface-recorded pattern-reversal VEP in the alert monkey. Vis Res 31:1143–1157.
Schroeder CE, Tenke CE, Givre SJ (1992) Subcortical contributions to the surface-recorded flash-VEP in the awake macaque. Electroenceph Clin Neurophysiol 84:219–231.
Schroeder CE, Steinschneider M, Javitt DC, Givre SJ, Mehta AD, Tenke CE, Simpson GV, Arezzo JC, Vaughan HG Jr (1994) Localization of ERP generators and identification of underlying neural processes. In: Perspectives of event-related potential research (EEG Suppl 44) (Karmos G, Czepe V, Czigler I, Desmedt JE, eds), pp. 55–75. Amsterdam: Elsevier.
Schroeder CE, Seto S, Arezzo JC, Garraghty PE. (1995) Electrophysiologic evidence for overlapping dominant and latent inputs to somatosensory cortex in squirrel monkeys. J Neurophysiol 74:722–732.
Schroeder CE, Javitt DC, Steinschneider M, Mehta AD, Givre SJ, Vaughan HG Jr, Arezzo, J. (1997a) NMDA-enhancement of phasic responses in primate neocortex. Exp Brain Res 114:271–278
Schroeder CE, Seto S, Garraghty PE (1997b) Emergence of radial nerve dominance in median nerve cortex after median nerve transection in an adult squirrel monkey. J Neurophysiol 77: 522–526
Shadlen MN, Newsome WT (1994) Noise, neural codes and cortical organization. Curr Opin Neurobiol 4:569–579.
Steinschneider M, Tenke CE Schroeder CE, Javitt DC, Simpson GV, Arezzo JC, Vaughan HG Jr (1992) Electroenceph Clin Neurophysiol 84:196–200.
Tanaka M, Lindsley E, Lausmann S, Creutzfeld OD (1990) Afferent connections of the prelunate visual association cortex (Area V4 and DP). Anat Embryol 181:19–30.
Tenke CE, Schroeder CE (1990) A model of sublaminar and thalamocortical contributions to the surface VEP: implications for current source density (CSD) analysis. Soc Neurosci Abstr 16:569.
Tenke CE, Schroeder CE (1992) Estimating neural generator power and field closure from intracranial current source density (CSD) profiles. Soc Neurosci Abstr 18:334.
Tenke CE, Schroeder CE (1994) The generator question: a comparison of event related potential (ERP) profiles with reconstructions from current source density (CSD) analysis. Soc Neurosci. Abstr 20:1000.
Tenke CE, Schroeder CE, Arezzo JC, Vaughan HG Jr (1993) Interpretation of high resolution current source density profiles: a stimulation of

sublaminar contributions to the visual evoked potential. Exp Brain Res 94:183–192.

Ungerleider LG (1995) Functional brain imaging studies of cortical mechanisms for memory. Science 270:769–775.

Ungerleider LG, Mishkin M (1982) Two cortical visual systems. In: Analysis of visual behavior (Ingle DJ, Goodale MA, Mansfield RJW, eds). Cambridge, MA: MIT Press.

Van Essen DC, Anderson CH, Felleman DJ (1992) Information processing in the primate visual system: an integrated systems perspective. Science 255:419–423.

Victor JD, Purpura KP (1996) Nature and precision of temporal coding in visual cortex: a metric-space analysis. J Neurophysiol 76:1310–1326.

Vogels R, Orban GA (1991) Quantitative study of striate single unit responses in monkeys performing an orientation task. Exp Brain Res 84:1–11.

Yoshida K, Benevento LA (1981) The projection for the dorsal lateral geniculate nucleus of the thalamus to the extrastriate visual association cortex in the macaque monkey. Neurosci Lett 22:103–108.

Yukie M, Iwai E (1981) Direct projection from the dorsal lateral geniculate nucleus to the prestriate cortex in macaque monkeys. J Comp Neurol 20:81–87.

Yukie M, Umitsu Y, Kido S, Niihara T, Iwai E (1979) A quantitative study of the cells projecting from the lateral geniculate nucleus to the prestriate cortex of the monkey with horseradish peroxidase. Neurosci Lett 13(Suppl 2):44.